FEEDFORWARD / FEEDBACK CONTROL OF AN INVERTER-BASED COMPENSATOR

By

Milton David Castro Núñez

A Thesis

Submitted to the Faculty of Graduate Studies
in partial fulfillment of the requirements for the degree of

Master of Science

The Department of Electrical and Computer Engineering

The University of Manitoba

Winnipeg, Manitoba, Canada

THE UNIVERSITY OF MANITOBA

FACULTY OF GRADUATE STUDIES

*****

COPYRIGHT PERMISSION PAGE

Feedforward / Feedback Control of an Inverter-Based Compensator

BY

Milton David Castro Núñez

A Thesis/Practicum submitted to the Faculty of Graduate Studies of The University of Manitoba in partial fulfillment of the requirements of the degree of Master of Science

Abstract

This research presents seven different control strategies for an inverter-based compensator used to achieve fast-acting reactive current compensation. Two feedforward schemes and five feedforward/feedback structures are analyzed. The first feedforward configuration uses phase-shift control (or simply δ-control) and results from shifting the fundamental component of a fixed pulse-width square wave an angle δ with respect to the sinusoidal network voltage. The second feedforward scheme uses phase-shift/pulse-width control (or simply δ/μ-control) and allows, in addition to the phase-shift, a variation of the pulse-width parameterized by μ. One feedforward/feedback scheme uses phase-shift control and the remaining feedforward/feedback schemes use phase-shift/pulse-width control.

A linearized average model that only considers the fundamental components of the circuit variables, and an exact model that takes into account all the non-linearities of the system are developed. The former model is suitable for control synthesis and stability analysis while the latter is used to benchmark the average model and to evaluate the effect of neglecting the higher-order harmonics.

All the control structures are examined in dynamic conditions by analyzing the transition from a capacitive to inductive mode of compensation, and vice-versa. The feedforward structures are also evaluated under stationary conditions in inductive and capacitive compensation modes. The performance achieved by each control strategy is evaluated by examining the compensator's dynamic response, using performance measures. The simulation results indicate that the variation of the pulse-width enables keeping a constant link voltage, and that the best performance is achieved with the δ/μ feedforward /Is-feedback to δ control.

Acknowledgments

I wish to express my sincere gratitude to Dr. Brian Perkins for his helpfulness during one of the most difficult times in my life. His excellent advice, support, guidance and supervision were crucial in making this seven-year dream a reality. I am deeply grateful, especially for his encouragement and help when I was about to surrender.

I owe a special debt of gratitude to Dr. Peter McLaren for his considerable respect for my culture and me, for his kindness and excellent lectures during the Power System Protection course. Dr. McLaren, thank you for your respectful treatment! I also extend my gratitude to Dr. Steve Onyshko. I greatly appreciate the technical assistance provided by Mr. Irwin Dirks.

I also must thank my father, Robinson Castro, the man who has brought me this far on his shoulders and who has devoted his life to his wife and children. My mother Olga, has also been the stone who supports me in my moments of weakness. I thank Jaime, my brother and my source of motivation and my sisters Tania and Glenna for their continuous inspiration.

I am grateful to Albert Epp and his wife, my host family in Canada as well as Dr. Donald Stewart for his counseling, which taught me to be more assertive and to value myself. My dear friends Eilef, Erik, Gratton, Debbie, Magne, Veronica, Vanya, Kin, Juan Carlos and all my colleagues at the power tower also deserve a special thank you gratitude for giving me an enjoyable social life.

I certainly appreciate the emotional support I have received from my friends in Colombia during my early days here.-- Beatriz, "gracias amiga", Vicky, Gloria C, Olga C, Cristina H, Eduardo, Maria P. "mi muñeca linda", Juan KK, Mauricio M, Jorge C, Jovan C, Jose A, Oscar S, Claudia B "la otra muñeca linda", Gilberto Giraldo "Gracias por tus excelentes concejos", Jorge D, Mónica C, Luis Giraldo, "llegue a considerar que mi amistad era valiosa para ti" and Jaime Blandón the manager of IEB consultants. My Thanks you to all of you for your emotional support, especially for the letter on Friday, December 18 1998. I still keep it!

Finally and most important, I want to thank my gorgeous princess Cinthya Parra, the woman who made me believe in love again, the sweetheart behind my success, the woman who brought serenity to my stormy days, light to my darkness, company to my solitude and love to my heart. "Princesita, siempre te amaré!"

Milton David Castro Núñez.

TABLE OF CONTENTS

CHAPTER 1

INTRODUCTION

1.1 Background

The investigation of feedforward-feedback control of an inverter-based compensator evolves from a previous investigation developed by [1]. In this research, an approximate linearized model was developed in order to characterize the fundamental frequency behaviour of the compensator. This average model uses one parameter of control, denominated as δ, and represents a phase shift between the network voltage and the fundamental component of the inverter voltage. The control algorithm installed on the actual laboratory prototype was implemented using a TMS320C30 digital signal processor. The experimental results of [1] showed that the approximate average model represented very well the fundamental frequency behaviour of the laboratory prototype under stationary and dynamic conditions. Nevertheless, one of the problems found by [1] in the laboratory prototype was the inability of the compensator to maintain a unique constant value for the link voltage in all the operability range of δ.

1.2 Expansion

The present investigation explores strategies to overcome some of the problems encountered in the compensator built by [1]. It also extends the theoretical knowledge about the behaviour in stationary and dynamic conditions of the actual laboratory prototype and explains in greater detail the results achieved by [1]. The drawbacks encountered in the previous research are overcome by including one more variable of control. Since the system is modeled not only by considering the fundamental frequency components, but also by using other mathematical techniques that make no approximation, the results achieved with the latter model validate the results obtained with the former. Furthermore, when the parameters and control strategies of the resultant exact mathematical model are set equal to the actual laboratory prototype, the theoretical results achieved with the former model agree with the results of the compensator developed by [1]. This investigation expands the previous research in the following topics:

- Implication of including another variable of control.
- Development of an exact model considering all the non-linearities of the system.
- Development of general dynamic transfer functions from the average model.
- Detailed root locus analysis of the dynamics transfer functions.
- Analysis of seven different controls structures.
- Determination of best instant for current and voltage sampling.
- Development of equations to find the appropriate current and voltage reference values
- Variable correlation between the exact and the linearized average model.

1.2.1 Implication of Another Control Variable

The control scheme of the compensator studied in the previous work only used one variable of control; therefore, only a feedforward phase-shift and feedforward/feedback phase-shift control scheme were analyzed and implemented. The modelling in the present work involves two variables of controls: One variable parameterized by μ that permits width variations of the square wave; the second variable parameterized by δ allows a phase-shift between the fundamental component of a square wave and the sinusoidal network voltage. The use of the latter variable alone yields to a phase-shift control strategy while the use of the two variables yields to a phase-shift/pulse-with control strategy. The last type of control permits the investigation of another variable in the behaviour of the compensator in dynamic and stationary conditions. It also gives different alternatives for control schemes depending on the feedback loop signal.

1.2.2 Development of an Exact Model and General Dynamic Transfer Functions

In order to validate the results of the approximate linear, time-invariant LTI continuous-time model, an exact model that considers all the non-linearities of the system is developed. The mathematical development involves calculation of convolutions requiring computer numerical compilations. Even though, the answer from this model is precise, it is not useful for control synthesis. On the other hand, the average model is not precise but permits the application of conventional control theory and it also allows state-space representation. This mathematical representation of a multiple-input, multiple-output system permits the development of several dynamic transfer functions, which facilitates the analysis of the system by examining the resultant single-input, single-output systems

1.2.3 Detailed Root Locus Analysis

The behaviour of a control system can only be understood with the appropriate control tool. Among the techniques available, the root locus method is simple, accurate and precise for the present analysis. The method is used to accomplish the following:

- Obtain the critical and optimal gain of the system.
- Determine the dynamics of the system as the control variables are changed in all their operability range.
- Comprehend the behaviour of the compensator in all its modes of operations.
- Resolve the dynamics of the closed-loop poles for a given optimal gain.
- Predict when possible, the response of the system to step changes in reactive current from one mode of operation to another.

1.2.4 Control Strategies

Feedforward and feedforward/feedback controls are the two main control schemes of the present research. The feedforward control structures are analyzed using two strategies: the phase-shift control with μ held constant at 120°, and the phase-shift/pulse-width control. The feedforward/feedback schemes are analyzed using feedback voltage loop and feedback current loop. Four of these structures are analyzed using of phase-shift/pulse-width control and one using phase-shift control with μ held constant at 120°. In all cases, a proportional control law is implemented.

1.2.5 Signal Sampling Issues and Reference Values.

One of the problems encountered in the preceding research was how to calculate the reference voltage value for the laboratory prototype. This problem was solved by a piecewise linearization of a nonlinear experimental curve [1]. The present investigation presents precise equations to calculate the reference voltage and current values for the exact model. This model is used to represent the actual laboratory prototype. It also analyzes the consequences of sampling at the wrong time and suggests the appropriate criteria to overcome this particular problem.

1.2.6 Model Correlation

Throughout this research, the correlation between the exact and the linearized average model is discussed. These correlations include, among others, the relationship between the input parameter values of the two models, reference values and step response. Due to the solution dependency on software packages of the exact model, in many cases the equations of the linearized average model facilitate finding new and less difficult expressions for the exact model. In other cases, the development of these expressions are found by solving, first, the equations of the exact model with the aid of computer programs and later finding analytical expressions to match the results.

1.3 Thesis Objectives

The main objectives of the present investigation are as follows:

- A solution to overcome the wide link voltage fluctuation of the inverter-based compensator developed in [1], when submitted to step changes in reactive current.

- An analysis of different feedforward and feedback controls.
- A determination of the best control strategy using performance measures such as, percent overshoot, time to rise, time to peak, steady state error and settling time.

1.4 Outline of the Thesis

A brief introductory chapter provides the background, the objectives of the thesis and an enlargement of the work in comparison to the previous investigation.

Chapter Two describes the mathematical modelling of the compensator using two different approaches. The resulting linearized average model uses basic circuit theory, Fourier analysis, linearization methods and state-space representation. On the other hand, the exact model relies on the mathematical solution of the systems' vector differential equations.

The feedforward control strategies are analyzed in Chapter Three. Two strategies are analyzed: the δ-feedforward control and the δ/μ feedforward control. The chapter ends by showing the correlation between the exact and the average model in terms of the variable μ.

In Chapter Four, the performance of the compensator, using voltage feedback loops is analyzed. The three strategies implemented in the exact and the average model are the δ-feedforward /U_o-feedback control with μ=120, the δ/μ-feedforward /U_o-feedback to δ control and the δ/μ-feedforward /U_o-feedback to μ control. All the control structures

involve the determination of the optimal control gain through root locus analysis. The expressions to calculate the voltage reference values for the exact model are also developed in this section. The system response is analyzed under stationary and dynamic conditions and the performance measures are estimated by submitting the compensator to step changes in reactive current.

In Chapter Five, the performance of the compensator using current feedback loops is analyzed. The two strategies implemented in the exact and the average model are the δ/μ-feedforward $/I_s$-feedback to δ control and the δ/μ-feedforward $/I_s$-feedback to μ control. All the control structures involve the determination of the optimal control gain through root locus analysis. The expressions to calculate the current reference values for the exact model are also developed in this section. The system response is analyzed under stationary and dynamic conditions and the performance measures are estimated by submitting the compensator to step changes in reactive current.

Chapter 6 provides the conclusions of the investigation and presents material for future work.

CHAPTER 2

SYSTEM MODELLING

2.1 System Description

The switching sequence used to generate the 3-level voltage waveform, depicted in Figure 2.1 as u_s, is achieved by means of generic switching elements represented in the graph as S_1, S_2, S_3, and S_4. C_o, U_n, L_s and R_s symbolize the other circuit parameters such as the dc capacitance, the network voltage, the inverter-coupling inductance and its associated resistance, respectively. The amplitude of the inverter voltage u_s is determined by the capacitor voltage U_o, and the input parameters δ and μ. The former parameter is the phase angle between the fundamental component of u_s and the network voltage U_n. The parameter μ is the width of the ac square wave generated by the switching devices. φ_1 and φ_2 fully determine the shape of the link voltage u_s. They also integrate the input parameters δ and μ.

The main objective of the present work is to investigate the controls of an inverter-based compensator with the aid of the conventional control theory. Thus, in order to apply the control concepts, the system is modeled only using the fundamental components of the circuit variables. Nevertheless, the resulting average model does not take into account the non-linearities; therefore an exact model that considers all the non-linearities of the system is also developed. The exact model is used to evaluate the effects of neglecting the high order harmonics and to benchmark the results of the control strategies obtained with the average model.

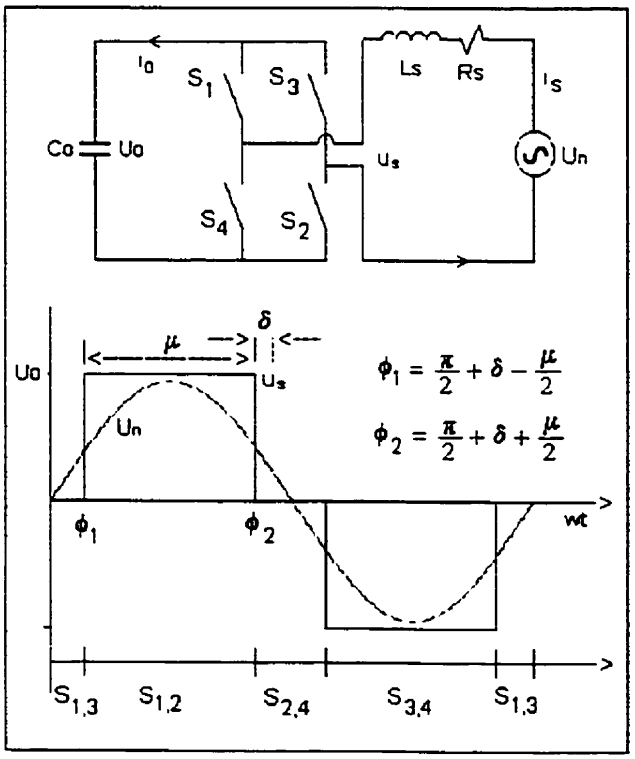

Figure 2.1. Circuit model of a single-phase inverter based compensator.

2.2 System Equations

The steady-state operation of the system comprehends a cyclic process determined by the switching scheme. When the switches S_1 and S_3 conduct, it can be seen from Figure 2.1 that the system can be described by the following equations:

$$L_s \frac{di_s}{dt} = -R_s i_s + u_n \tag{2.1}$$

$$0 = C_o \frac{du_o}{dt} \tag{2.2}$$

When the switches S_1 and S_2 conduct, the system equations become:

$$L_s \frac{di_s}{dt} = -R_s i_s - u_o + u_n \tag{2.3}$$

$$i_s = C_o \frac{du_o}{dt} \tag{2.4}$$

The other combinations of switching states described in Figure 2.1 (S_{24} and S_{34}) yield respectively to either the first set of equations or to the second set. Therefore, the system can be described in terms of the circuit parameters by the following expressions:

$$L_s \frac{di_s}{dt} = -R_s i_s - u_s + u_n \tag{2.5}$$

$$i_o = C_o \frac{du_o}{dt} \tag{2.6}$$

Here the state of the switching sequence in conjunction with U_o and i_s determines the value of u_s and i_o.

2.3 Average Model

In order to apply the control theory and to investigate the stationary and dynamic behaviour of the system, an average model will be developed. The first step of this process is to find the fundamental component of the ac square wave formed by the switching devices depicted in Figure 2.1.

The expression for the fundamental component of the inverter voltage is as a function of δ and μ, as follows.

$$< U_s(t) >_1 = \frac{4U_o}{\pi} sin\left(\frac{\mu}{2}\right) sin(\omega t - \delta) \tag{2.7}$$

The application of Kirchoff's current law yields the expression for the fundamental component of the current, denoted by $<i_s>_1$.

$$< i_s(t) >_1 = \left[\frac{4U_o}{\pi\sqrt{R_s^2 + \omega^2 L_s^2}} sin(\frac{\mu}{2}) \cos(\delta + \varphi)\right] sin(\omega t) + \left[\frac{4U_o}{\pi\sqrt{R_s^2 + \omega^2 L_s^2}} sin(\frac{\mu}{2}) sin(-\delta - \varphi)\right] \cos(\omega t) \tag{2.8}$$

Where:

$$\varphi = \tan^{-1}(\frac{\omega L_s}{R_s})$$

Equation 2.8 can be expressed as follows:

$$< i_s(t) >_1 = I_{11} sin(\omega t) + I_L \cos(\omega t)$$

(2.9)

This result shows that the current can be expressed as the summation of two components: one in parallel with the network voltage and the other one in quadrature. It is convenient to denote these currents as I_{11} for the former and I_L for the latter. I_{11} can be thought as the active current and I_L as the reactive current.

Taking the derivative of Equation (2.19), equating the result with expression (2.5) and collecting common terms in sin(ωt) and cos(ωt), yields the following non-linear differential equations.

$$\frac{dI_{11}}{dt} = -\frac{R_s}{L_s} I_{11} + \omega I_L - \frac{4Uo}{\pi L_s} \sin(\frac{\mu}{2}) \cos(\delta) + \frac{u_n}{L_s}$$

(2.10)

$$\frac{dI_L}{dt} = -\omega I_{11} - \frac{R_s}{L_s} I_L + \frac{4Uo}{\pi L_s} sin(\frac{\mu}{2}) sin(\delta)$$

(2.11)

Analyzing the behaviour of the capacitor permits the development of expression for the capacitor voltage. Averaging the power delivered into the inverter terminals and dividing by the dc component of U_o results in the following expression.

$$\frac{P_{av}}{U_o} = \frac{2}{\pi} \sin\left(\frac{\mu}{2}\right) [I_{11} \cos(\delta) - I_L \sin(\delta)]$$

(2.12)

The above equation determines the average current into the capacitor, but this current can also be found with the following well-known equation:

$$i_o = C_o \frac{dU_o}{dt} \tag{2.13}$$

Combining Equation (2.12) and (2.13) yields the following expression:

$$\frac{dU_o}{dt} = -\frac{2}{C_o \pi} \sin(\frac{\mu}{2}) [I_{11} \cos(\delta) - I_L \sin(\delta)] \tag{2.14}$$

The average model is now fully represented by Equations (2.10), (2.11) and (2.14). While the equations determine the behaviour of the compensator, it is described by a set of non-linear differential equations; therefore, a linearized average model must be developed in order to apply the conventional control theory.

2.4 Stationary Solution

In steady state, at any given operating point associated with the parameters δ^* and μ^* the terms dI_{11}^*/dt, dI_L^*/dt and dU_o^*/dt, of Equations (2.10), (2.11) and (2.14) respectively, are equal to zero. This yields a system described by a set of 3 equations and 3 unknowns. Solving the resultant system yields the steady state operating point of the single-phase inverter based compensator.

$$I^*_{11} = \frac{U_n}{2R_s} [1 - \cos(2\delta^*)] \tag{2.15}$$

$$I^*_L = \frac{U_n}{2R_s}\sin(\delta^*) \tag{2.16}$$

$$U^*_o = \frac{U_n}{4\sin(\frac{\mu^*}{2})}\frac{\cos(\varphi - \delta^*)}{\cos(\varphi)} \tag{2.17}$$

Equations (2.15) and (2.16) show that both the active and the reactive current are independent of the parameter μ. On the other hand, expression (2.17) shows that the voltage is a function of both parameters, δ and μ.

2.5 Linearized Average Model

So far the system has been described by Equations (2.10), (2.11) and (2.14). All these expressions are functions of the active current I_{11}, the reactive current I_L, the capacitor voltage U_o and the input parameters δ and μ. These equations are repeated here for convenience.

$$\frac{d\tilde{I}_{11}}{dt} = -\frac{R_s}{L_s}I_{11} + \omega I_L - \frac{4Uo}{\pi L_s}\sin(\frac{\mu}{2})\cos(\delta) + \frac{u_n}{L_s} = f(I_{11}, I_L, U_o, \delta, \mu) \tag{2.18}$$

$$\frac{d\tilde{I}_L}{dt} = -\omega I_{11} - \frac{R_s}{L_s}I_L + \frac{4Uo}{\pi L_s}\sin(\frac{\mu}{2})\sin(\delta) = f(I_{11}, I_L, U_o, \delta, \mu) \tag{2.19}$$

$$\frac{d\tilde{U}_o}{dt} = -\frac{2}{C_o\pi}\sin(\frac{\mu}{2})\left[I_{11}\cos(\delta) - I_L\sin(\delta)\right] = f(I_{11}, I_L, U_o, \delta, \mu) \tag{2.20}$$

Since there is no general theory for the analysis and design of non-linear systems and it is clear that the above is non-linear, it is necessary to obtain a linear model. The linearization around an operating point can be found by obtaining the Jacobian of the system, which bears the following results.

$$\mathbf{A}=\begin{bmatrix} -\frac{R_s}{L_s} & \omega & -\frac{4}{\pi L_s}\sin(\frac{\mu^*}{2})\cos(\delta^*) \\ -\omega & -\frac{R_s}{L_s} & \frac{4}{\pi L_s}\sin(\frac{\mu^*}{2})\sin(\delta^*) \\ \frac{2}{\pi C_o}\sin(\frac{\mu^*}{2})\cos(\delta^*) & -\frac{2}{C_o\pi}\sin(\frac{\mu^*}{2})\sin(\delta^*) & 0 \end{bmatrix}$$

Notice that the elements of this matrix are formed by circuit variables and/or the input parameters δ and μ. It is also convenient to note that the variables I_{11} I_L and U_o are not part of the elements of this matrix.

$$\mathbf{B}=\begin{bmatrix} \frac{4U^*_o}{\pi L_s}\sin(\frac{\mu^*}{2})\sin(\delta^*) & -\frac{2U^*_o}{\pi L_s}\cos(\delta^*)\cos(\frac{\mu^*}{2}) \\ \frac{4U^*_o}{\pi L_s}\sin(\frac{\mu^*}{2})\cos(\delta^*) & \frac{2U^*_o}{\pi L_s}\sin(\delta^*)\cos(\frac{\mu^*}{2}) \\ \frac{2}{\pi C_o}\sin(\frac{\mu^*}{2})\left[-I^*_{11}\sin(\delta^*)-I^*_L\cos(\delta^*)\right] & \left[I^*_{11}\cos(\delta^*)-I^*_L\sin(\delta^*)\right]\frac{\cos(\frac{\mu^*}{2})}{\pi C_o} \end{bmatrix}$$

The above result shows that, unlike matrix **A**, the elements of matrix **B** involve circuit variable, input parameters and the variables I_{11}, I_L and U_o.

An analysis of Equations (2.18), (2.19) and (2.20) in conjunction with the Jacobian permits the representation of the system by the state space form.

$$\frac{d}{dt}\begin{bmatrix}\tilde{I}_{11}\\ \tilde{I}_L\\ \tilde{U}_o\end{bmatrix} = \mathbf{A}\begin{bmatrix}\tilde{I}_{11}\\ \tilde{I}_L\\ \tilde{U}_o\end{bmatrix} + \mathbf{B}\begin{bmatrix}\tilde{\delta}\\ \tilde{\mu}\end{bmatrix} \tag{2.21}$$

Where $\tilde{I}_{11}$ represents the perturbation from stationary conditions (I^*_{11}), similarly for $\tilde{I}_L$ and $\tilde{U}_o$.

2.6 Dynamic Transfer Functions

The state-space model represented by Equation (2.21) describes a multiple input, multiple output system where the perturbed state variables $\tilde{I}_{11}$, $\tilde{I}_L$ and $\tilde{U}_o$ form the state vector and the perturbed input parameters $\tilde{\delta}$ and $\tilde{\mu}$ compose the control vector. δ And μ will be also referred to as the control parameters. The system's transfer function matrix is:

$$\begin{bmatrix}G_{11}(s) & G_{12}(s) & G_{13}(s)\\ G_{21}(s) & G_{22}(s) & G_{23}(s)\\ G_{31}(s) & G_{32}(s) & G_{33}(s)\end{bmatrix} = (SI - A)^{-1}B$$

The elements of this matrix relate the state variables with the control parameters $\tilde{\delta}$ and $\tilde{\mu}$. For instance, the element $G_{21}(s)$ relates the state variable $\tilde{I}_L$ and the control parameter $\tilde{\delta}$, while the element $G_{22}(s)$ relates $\tilde{I}_L$ and $\tilde{\mu}$. The capacitor voltage is related

to the parameter parameters $\delta^{\sim}$ and $\mu^{\sim}$ through the elements $G_{31}(s)$ and $G_{32}(s)$. The following are the two last rows of the matrix operation described above.

$$G_{21}(s)=\frac{\tilde{I}_L(s)}{\tilde{\delta}(s)}=\frac{-K_1\left[-(K_3Y_S\cos\delta^*)s^2+(K_3Y_S\sin\delta^*-K_3R_S\cos\delta^*+K_1I_1Y_S\sin\delta^*)s-U_0K_1^2\cos\delta^*+K_1I_1R_S\sin\delta^*+K_1I_1Y_S\cos\delta^*\right]}{2Y_S^2B_0s^3+4Y_SB_0R_Ss^2+(K_1^2Y_S+2Y_S^2B_0+2B_0R_S^2)s+R_SK_1^2} \tag{2.22}$$

$$G_{22}(s)=\frac{\tilde{I}_L(s)}{\tilde{\mu}(s)}=\frac{-\frac{K_2}{2}\left[(K_3Y_S\sin\delta^*)s^2+(K_3Y_S\cos\delta^*+K_3R_S\sin\delta^*+K_1I_2Y_S\sin\delta^*)s+K_1I_2R_S\sin\delta^*+K_1I_2Y_S\cos\delta^*\right]}{2Y_S^2B_0s^3+4Y_SB_0R_Ss^2+(K_1^2Y_S+2Y_S^2B_0+2B_0R_S^2)s+R_SK_1^2} \tag{2.23}$$

$$G_{31}(s)=\frac{\tilde{U}_0(s)}{\tilde{\delta}(s)}=\frac{-K_1\left[(Y_S^2I_1)s^2+(2Y_SR_SI_1)s+(Y_S^2+R_S^2)I_1-K_1U_0Y_S\right]}{2Y_S^2B_0s^3+4Y_SB_0R_Ss^2+(K_1^2Y_S+2Y_S^2B_0+2B_0R_S^2)s+R_SK_1^2} \tag{2.24}$$

$$G_{32}(s)=\frac{\tilde{U}_0(s)}{\tilde{\mu}(s)}=\frac{\frac{K_2}{2}\left[(I_2Y_S^2)s^2+(2I_2Y_SR_S-K_1U_0Y_S)s+(Y_S^2+R_S^2)I_2-K_1U_0R_S\right]}{2Y_S^2B_0s^3+4Y_SB_0R_Ss^2+(K_1^2Y_S+2Y_S^2B_0+2B_0R_S^2)s+R_SK_1^2} \tag{2.25}$$

where,

$$I_1=I_{11}\sin\delta+I_L\cos\delta$$

$$I_2=I_{11}\cos\delta-I_L\sin\delta$$

$$K_1=\frac{4}{\pi}\sin(\frac{\mu}{2}) \qquad K_2=\frac{4}{\pi}\cos(\frac{\mu}{2}) \qquad K_3=2U_0B_0$$

$$B_0=\omega C_0$$

The above set of Equations (2.22) to (2.25) describes the dynamic transfer functions of the system. It can be seen that they all have the same denominator. This result shows that the open-loop poles of all these transfer functions are the same. Each one of these transfer functions will be the base of the control structure in later chapters. The applicability of each control structure will be determined by analyzing the behaviour of the compensator when submitted to step changes in the reactive current set point.

2.7 Exact Model

For any power electronic circuit model consisting of interconnections of linear, time-invariant (LTI) elements, ideal switches and ideal sources, it is straightforward to obtain an exact mathematical representation of the evolution of the state variables describing the circuit. [2]. An analysis to Figure 2.1 permits the determination of the evolution of the state variables of the circuit. This progress can be found with the aid of Figure 2.2, which describes the system's states evolution. It can be seen that the circuit alternates between two states and that due to the switching sequence, it is sufficient to analyze a complete half cycle determined by the interval $0< \omega t <\pi$. During this interval the system progresses through two distinct states, represented in the graph by SB1 and SB2. State SB1 is defined in the sub-interval $0< \omega t < \varphi_1$, while State SB2 is defined in the sub-interval $\varphi_1< \omega t < \varphi_2$.

Using the fact that power electronic circuits are designed in a way that preserves continuity of the state variables, the final state in the i-th configuration becomes the initial state for the (i+1)-th configuration. [2]. Considering the cyclical behaviour of the

system, it is straightforward to fully analyze the circuit using its two modes of operation and Equations (2.1), (2.2), (2.3) and (2.4).

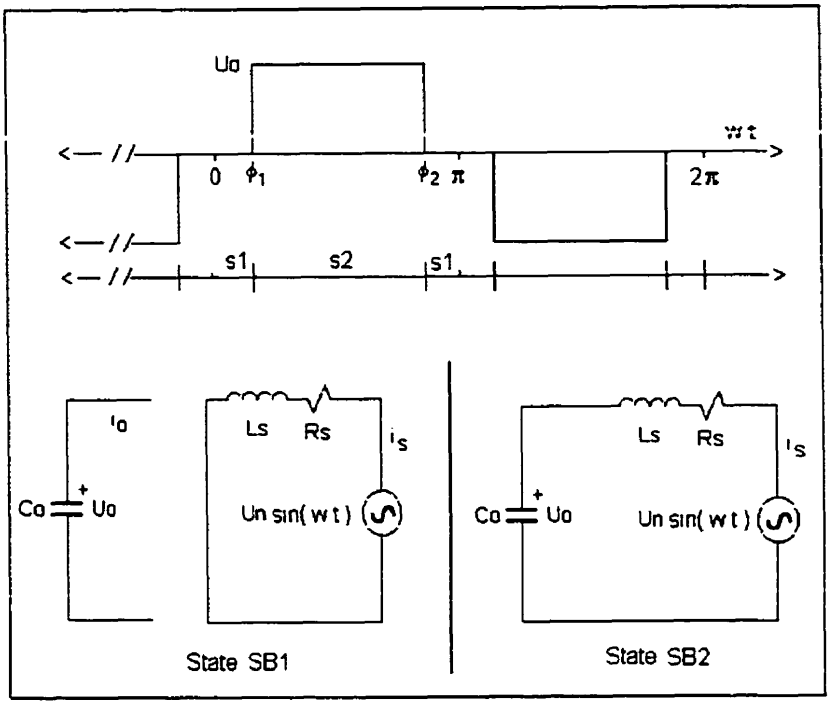

Figure 2.2. System evolutions according to the switching sequence.

The first mode of operation defined by the state SB1 is described by Equation (2.1) and (2.2). These equations allow the state-space representation given by the following expression:

$$\frac{d}{d(\omega t)}\begin{bmatrix} i_s \\ u_o \end{bmatrix} = \begin{bmatrix} -\frac{R_s}{X_s} & 0 \\ 0 & 0 \end{bmatrix}\begin{bmatrix} i_s \\ u_o \end{bmatrix} + \begin{bmatrix} \frac{1}{X_s} \\ 0 \end{bmatrix} u_n \tag{2.26}$$

Equation (2.26) has the solution given by:

$$\begin{bmatrix} i_s(\varphi_1) \\ u_o(\varphi_1) \end{bmatrix} = e^{\mathbf{A}_0(t1-t0)} * \chi(0) + \int_0^{\varphi_1} e^{\mathbf{A}_0(\varphi_1-\tau)} \mathbf{B}_0 u_n(\tau) d\tau \tag{2.27}$$

where,

$$\mathbf{A}_0 = \begin{bmatrix} -\frac{R_s}{X_s} & 0 \\ 0 & 0 \end{bmatrix}$$

$$\mathbf{B}_0 = \begin{bmatrix} \frac{1}{X_s} \\ 0 \end{bmatrix}$$

$\chi(0)$ denotes the initial condition of i_s and u_o.

The second mode of operation defined by state SB2 is described by Equation (2.3) and (2.4). These equations also allow the state-space representation given by the following expression:

$$\frac{d}{d(\omega t)} \begin{bmatrix} i_s(\varphi_2) \\ u_o(\varphi_2) \end{bmatrix} = \begin{bmatrix} -\frac{R_s}{X_s} & \frac{-1}{X_s} \\ \frac{1}{B_0} & 0 \end{bmatrix} \cdot \begin{bmatrix} i_s \\ u_o \end{bmatrix} + \begin{bmatrix} \frac{1}{X_s} \\ 0 \end{bmatrix} \cdot u_n \tag{2.31}$$

Equation (2.28) has the solution given by:

$$\begin{bmatrix} i_s(\varphi_2) \\ u_o(\varphi_2) \end{bmatrix} = e^{\mathbf{A}_1(t2-t1)} \chi(t_1) + \int_{t1}^{t2} e^{\mathbf{A}_1(t2-\tau)} \mathbf{B}_1 u_n(\tau) d\tau \tag{2.29}$$

where,

$$\mathbf{A}_1 = \begin{bmatrix} -\frac{R_s}{X_s} & \frac{-1}{X_s} \\ \frac{1}{B_0} & 0 \end{bmatrix}$$

$$\mathbf{B}_1 = \begin{bmatrix} \frac{1}{X_s} \\ 0 \end{bmatrix}$$

and $\chi(\varphi_1)$ denotes the initial condition of i_s and u_o at φ_1.

The system returns now to the first mode of operation, but this time the initial conditions are given at time φ_2. Therefore, the solution at the end of the interval is given by the following expression:

$$\begin{bmatrix} i_s(\pi) \\ u_o(\pi) \end{bmatrix} = e^{\mathbf{A}_0(\pi-\varphi_2)} \cdot \chi(\varphi_2) + \int_{\varphi 2}^{\pi} e^{\mathbf{A}_0(\varphi_2-\tau)} \mathbf{B}_0 u_n(\tau) d\tau \tag{2.34}$$

where,

$\chi(\varphi_2)$ denotes the initial condition of i_s and u_o at φ_2.

By piecing together the above solutions we can relate the extremes of the interval as fallows:

$$\chi(\pi) = \zeta \cdot \chi(0) + \xi \tag{2.31}$$

where,

$$\chi = (i_s \quad u_o)^T$$

$$\zeta = e^{A_0(\pi-\varphi_2)} . e^{A\ (\varphi_2-\varphi_1)} . e^{A_0(\varphi_1-0)} \tag{2.32}$$

$$\xi = e^{A_0(\pi-\varphi_2)} . \left\{ e^{A\ (\varphi_2-\varphi_1)} + \int_0^{\varphi_1} e^{A_0(\varphi_1-\tau)} \mathbf{B}_0 u_n(\tau) d\tau + \int_{\varphi_1}^{\varphi_2} e^{A_1(\varphi_2-\tau)} \mathbf{B}_1 u_n(\tau) d\tau \right\} + \int_{\varphi_2}^{\pi} e^{A_0(\varphi_2-\tau)} \mathbf{B}_0 u_n(\tau) d\tau \tag{2.33}$$

The values of φ_1 and φ_2 are determined by the control parameters δ and μ. Thus ζ and ξ are functions of δ and μ. At any permissible operating values of δ^* and μ^* it is possible to exploit the fact that under stationary conditions, i_s is an alternating current while the voltage across the capacitor is a dc voltage. It follows then, from Equation (2.31) that the value of the state variables at the endpoints of the interval are related by the following equation:

$$\chi^*(\pi) = \begin{bmatrix} -1 & 0 \\ 0 & 1 \end{bmatrix} \chi^*(0) \tag{2.34}$$

Substituting Equation (2.34) into (2.31) and solving for the state vector at 0, yields to the expression:

$$\chi^*(0) = \left(\begin{bmatrix} -1 & 0 \\ 0 & 1 \end{bmatrix} - \zeta^* \right)^{-1} . \xi^* \tag{2.35}$$

This mathematically rigorous approach makes no approximation and thus is generally applicable, even in systems where the assumptions made in obtaining the averaged model do not hold. [3]. Nevertheless, the solution is absolutely dependent on numerical packages like MATLAB.

CHAPTER 3

FEEDFORWARD CONTROL

3.1 Benchmark System Parameters

In this section the behaviour of the compensator is analyzed with the aid of the two models developed in Chapter 2. The models are tested under stationary and dynamic conditions. Two types of control strategy are implemented in each model--(i) the δ feedforward control developed also in a previous thesis, and (ii) the δ-μ feedforward control proposed in the present work.

In order to make a fair comparison between the two types, several performance measures are evaluated. The estimation of these performance measures is achieved by submitting the compensator to step changes in reactive current from inductive to capacitive and vice-versa. These measures show the performance of the compensator under dynamic conditions. Both models use the same circuit parameter values. The rating of the capacitor is Co=2400 μF, Uo=450 V. The reactor rating is Ls=10 mH, Xs/Rs=7.2; note

that the resistance is determined by the ratio Xs/Rs, which gives the quality factor of the inductor. The network voltage is set to have a fixed value of Un=√2*120 V and the system's frequency is assumed to be 60 Hz.

3.2 The δ - Feedforward Control

A close inspection of Equation (2.17) shows that holding μ and U_n constant indicates a relation between the variables δ and U_o. This means that as soon as δ is changed, the correspondent value of U_o is known. The knowledge of the amount of disturbance in advance suggests the use of feedforward control in order to reduce the transient error. The application of Equation (2.17) to the exact model will yield a response with an error that will be analyzed in the last section of this chapter.

3.2.1 Control Description

The control structure implemented in the exact and in the linearized average model is depicted in Figure 3.1. The upper scheme determines the control structure to be implemented in the exact model while the lower scheme depicts the control structure for the linearized average model. Matrix **A** corresponds to the Jacobian matrix of Chapter 2, with μ held constant at 120°. Matrix $\mathbf{B_d}$ is the first column vector of matrix **B** of Chapter 2, with μ held constant at 120°.

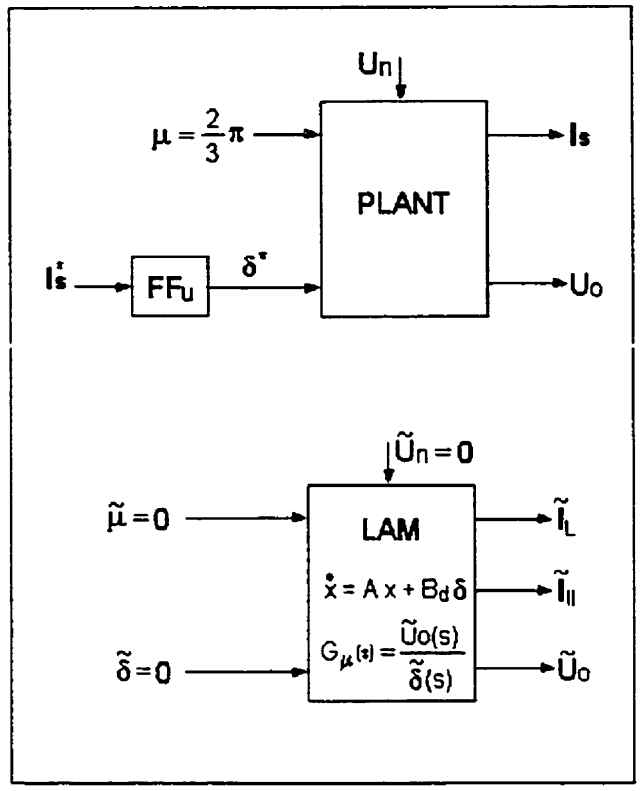

Figure 3.1. Feedforward (FF) control structures for the exact and linearized average model.

3.2.2 Stationary Behaviour

The behaviour of the compensator in inductive mode with δ = - 2° and μ = 120° is depicted in Figure 3.2. The solid line illustrates the result using the average model, (Equations 2.15 to 2.17,) while the solution achieved with the exact model, (Equation 2.35,) is described by a dotted line. The operation of the compensator in capacitive mode with δ = 2° and μ = 120° is also depicted in Figure 3.2. Both models show the dependency of the capacitor's voltage on the control parameter δ when μ is held constant at 120°. This dependency can be clearly seen with the aid of Equation (2.17) in Section 2.4, which shows that when μ and U_n are held constant, the capacitor voltage U_o is not

only uniquely dependent on δ but also directly proportional to $\cos(\varphi - \delta)$. Therefore, when $\delta<0$, the term $\cos(\varphi - \delta)$ is closer to 90° and the voltage decreases; on the other hand, when $\delta>0$, the term $\cos(\varphi - \delta)$ is closer to zero and thus the voltage increases. Figure 3.2 also shows how well the average model represents the fundamental frequency behaviour of the compensator in stationary conditions.

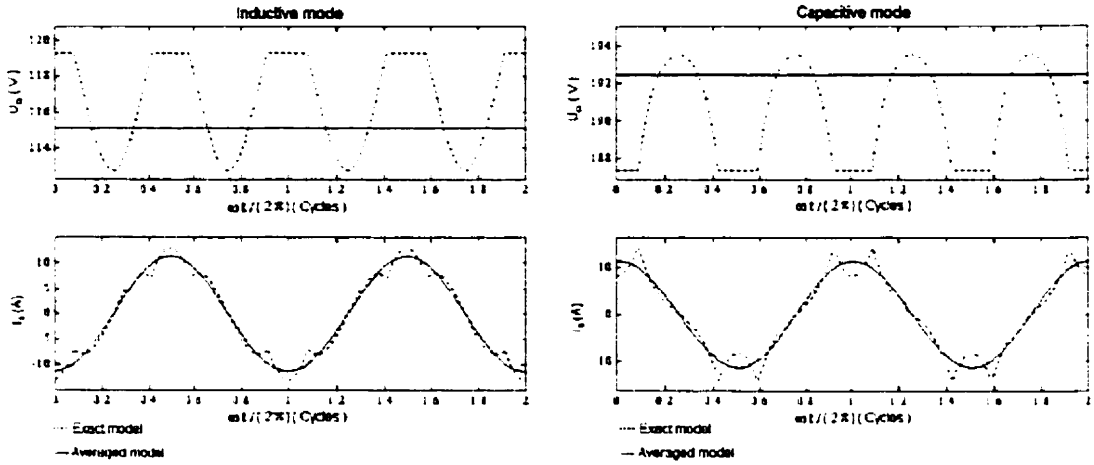

Figure 3.2 Stationary solutions for inductive mode (left) and capacitive modes (right), achieved with averaged model (solid line) and exact model (dotted line).

When the system is analyzed with the exact model, even though the fundamental component of the current is clearly a sinusoidal wave, regardless of the mode of operation, the shape of the system's current varies depending on the compensation mode. The difference in the shape of the current signal will become a key factor in the analysis of the control structures involving feedback current. It is also important to note that with the exact model, the voltage waveform changes as well, depending on the mode of compensation. Again, in the exact model, the difference in the shape of the capacitor dc voltage signal will be a key factor when analyzing control structures involving feedback voltage.

3.2.3 Dynamic Behaviour

The response of the compensator to a step change in current from 11.31 A peak inductive to 11.31 A peak capacitive, (holding μ constant at 120°) is depicted in Figure 3.3. The right side illustrates the response using the exact model, while the left describes the response of both models but highlights the response of the average model. The current evolution from inductive to capacitive mode is easily viewed on the graph by observing its 180 phase-shift.

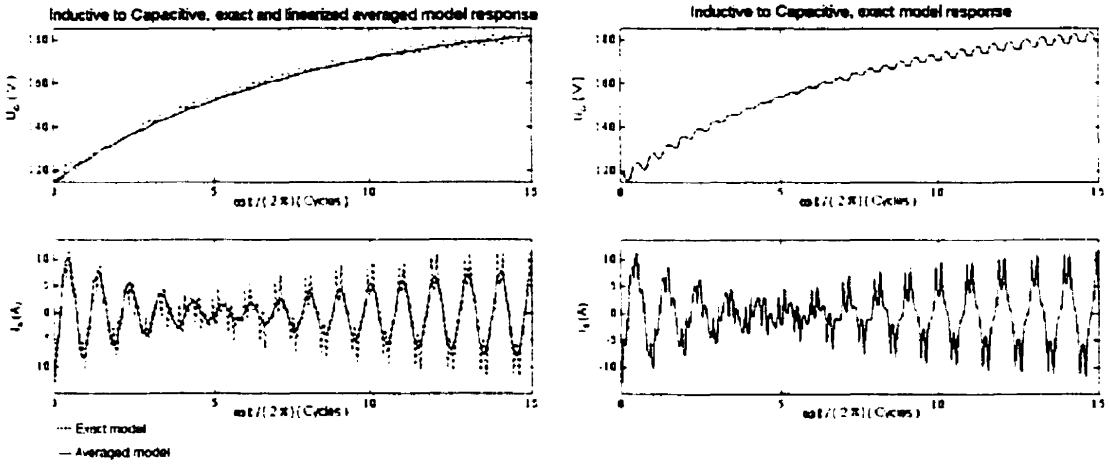

Figure 3.3 Dynamic behaviour to a step change in current from 11.3 A inductive to 11.311 A capacitive obtained with the average model (left) and with the exact model (right). (Step change in δ)

The response of the system for the inverse transition, this is, from inductive operation at δ = -2° to capacitive operation at δ = +2°, is described in Figure 3.4. Both figures highlight the voltage dependence of the system on the control parameter δ when μ is held constant at 120°. This voltage fluctuation not only forces the capacitor to operate at different voltage levels, but yields to voltage reference according to the value of the parameter δ.

Thus, in order to maintain the voltage U_o at a constant level, the parameter μ must enter into play.

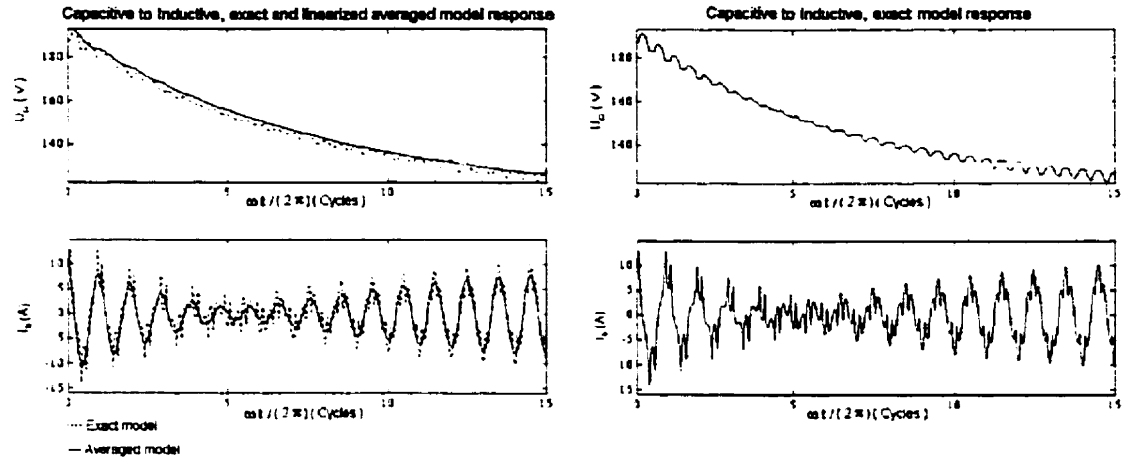

Figure 3.4. Dynamic behaviour to a step change in δ from +2° to -2° obtained with the exact and average model (left) and with the exact model (right).

3.2.4 Performance Measures

The progress of the reactive current during the transients from inductive to capacitive and vice-versa are depicted in Figure 3.5. This figure also shows the voltage transient across the capacitor. The performance measures associated with these step changes in reactive current are shown in Tables 1 and 2. Both tables show the performance measures for the transients related to the voltage and to the current. The first table is associated with the change from inductive to capacitive while the second is associated with the change from capacitive to inductive.

An important feature of this type of control encountered by [1] and verified in this section, is the voltage variation across the capacitor. In the present work, the inclusion of

the control parameter μ diminishes this voltage fluctuation, as will be seen in subsequent sections.

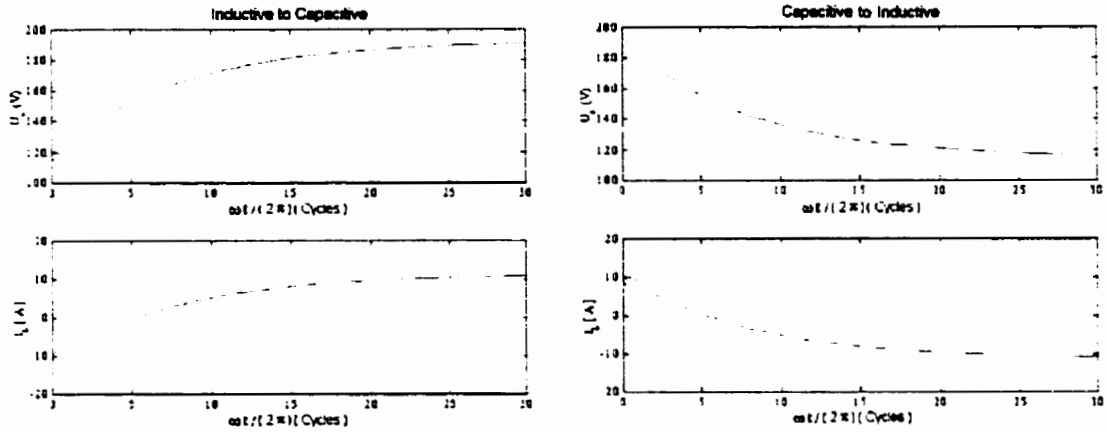

Figure 3.5. Step change in current from inductive to capacitive (left) and for capacitive to inductive (right).

Table 3.1 $\delta = -2°$ **to** $2°$ **and** $\mu = 120°$

VOLTAGE MEASURES		CURRENT MEASURES	
Time to rise [s]	0.281781	Time to rise [s]	0.278778
Settling time [s]	0.266266	Settling time [s]	0.469969
Steady-state error [%]	0.804986	Steady-state error [%]	3.967796

Table 3.2 $\delta = +2°$ **to** $-2°$ **and** $\mu = 120°$

VOLTAGE MEASURES		CURRENT MEASURES	
Time to rise [s]	0.282282	Time to rise [s]	0.277778
Settling time [s]	0.332332	Settling time [s]	0.469469
Steady-state error [%]	1.347399	Steady-state error [%]	3.940048

3.3 The δ / μ Feedforward Control

A close examination of Equation (2.17) shows that in order keep U_o at a constant value, the parameter in control μ must be allowed to change. This change yields a unique correspondence between δ and μ. But it also suggests again the use of feedforward control, since the undesired effect of the disturbance and its correction is known in advance. In this section, the value of μ for the exact model is found with the aid of Equation (2.17) and corrected using Equation (3.1) in Section 3.4

3.3.1 Control Description

The control structure implemented in the exact and in the linearized average model is depicted in Figure 3.6. The upper scheme determines the control structure implemented in the exact model while the lower scheme describes the control scheme implemented in the linearized average model. Notice that in the exact model the value of μ depends on the variable U_o^* and δ^*. Matrix **A** is the Jacobian matrix of the system evaluated with the proper values of δ and μ. Matrix $\mathbf{B_d}$ is the first column vector associated with Jacobian matrix **B**. G_{31} is the feedforward transfer function given by Equation (2.24).

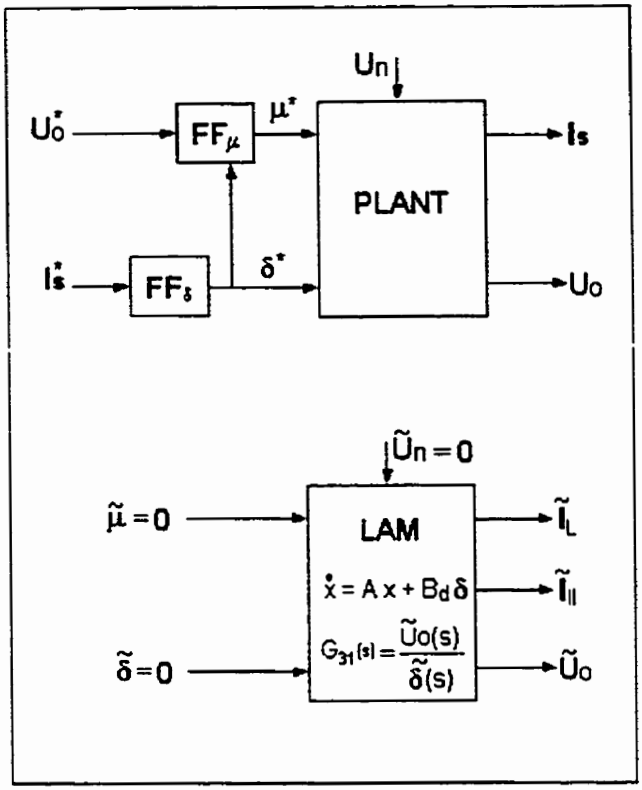

Figure 3.6. δ-μ Feedforward control schemes for the exact and the linearized average model.

3.3.2 Stationary Behaviour

The behaviour of the compensator with the δ-μ feedforward control, under stationary conditions is depicted in Figure 3.7. The first interesting result that comes to light is the ability of the compensator to maintain the voltage at a constant level, regardless of the mode of operation. The straight solid lines at 220 V on the upper graphs are associated with the results of the linearized average model, while the dotted lines are associated with the exact model; the effective voltage value of the response signal obtained with the exact model is exactly 220 V. Nevertheless, in the capacitive mode, the peak voltage is higher than in the inductive mode; therefore, care must be taken when defining the moment of sampling when implementing feedback current loops.

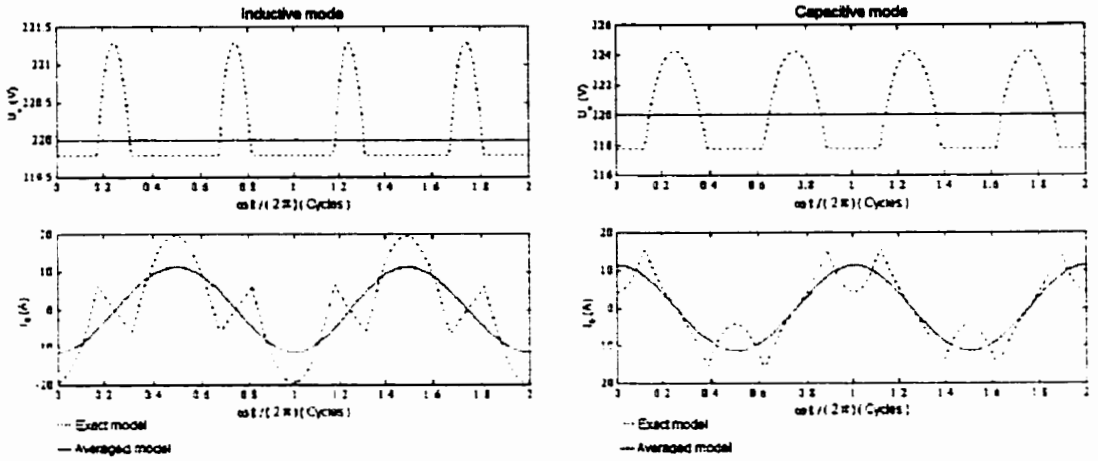

Figure 3.7. Stationary behaviour of the compensator in inductive mode (left) and in capacitive mode (right), obtained with the linearized average model (solid line) and with the exact model (dotted line).

The behaviour of the system's current is also depicted in Figure 3.7. It is clear from the average model response (i.e., solid line) that the control parameter μ has no influence on the current, as was expected from the mathematical results in Chapter 2. On the other hand, it is also clear from the exact model that the deviation of the control parameter μ from the value 120° increases the current harmonic content. Another interesting result associated with the exact model response is the difference in the peak current, which in inductive mode is about 20 A, while in capacitive mode is around 15 A. This difference is not small and thus it cannot be neglected. In general, in the inductive mode, the peak current is higher than in the capacitive mode. It will be shown in later chapters that there is a dependency between the parameter δ and the peak current

3.3.3 Dynamic Behaviour

The ability of the compensator to reduce the voltage fluctuation during a transition associated with a step change in current from inductive to capacitive (and vice-versa,)

when using the δ-μ feedforward control is depicted in Figure 3.8. The right side of the figure shows the exact response of the compensator to a change in current from 11.311 A peak inductive to 11.311 A peak capacitive. The left side shows the responses obtained with both models but highlights the linearized average model. The voltage drop in the capacitor can be explained with the aid of an RLC series circuit with a variable capacitance. In stationary conditions, the voltage across the capacitor and the reactor are fixed and their summation equals the network voltage. At the moment of the transition the capacitive component current is increased and the inductive component of the current is decreased. Since the current across the reactor is not allowed to change immediately, the storage flux creates an electromagnetic force in order to maintain the inductive current constant. This emf adds to the steady-state voltage across the reactor, thus causing an increment in the voltage across the reactor and therefore a reduction in the capacitor voltage. As the electromagnetic force decreases the voltage across the reactor decreases and the voltage across the capacitor increases. These process takes places until the emf is zero and the steady state is reached again.

The 180° phase-shift in the current permits the observation of the evolution of the transient from inductive to capacitive; but unlike the response obtained with the δ-feedforward control, the peak current does not reduce during the transient.

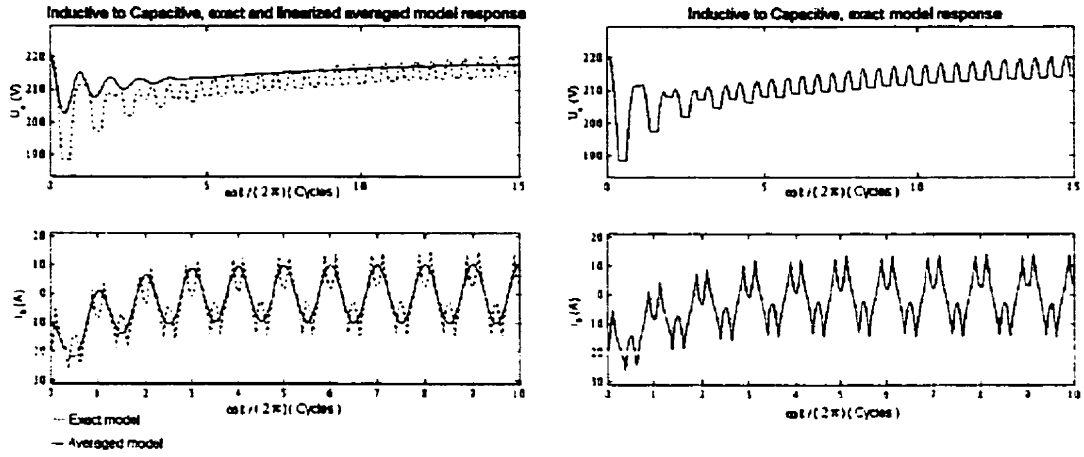

Figure 3.8. Dynamic responses of the compensator to a step change in current from 11.31 A peak inductive to 11.31 A peak capacitive, achieved with the average model (left) and the exact model (right).

The response of the compensator to the inverse step change in current is depicted in Figure 3.9. The voltage increment can also be explained with the aid of an RLC series circuit. In this case, the compensator is working in capacitive mode and in the inductive component the current is increased; this increase causes a reduction in the voltage across the inductor due to the storage flux and therefore causes an increment in the capacitor voltage.

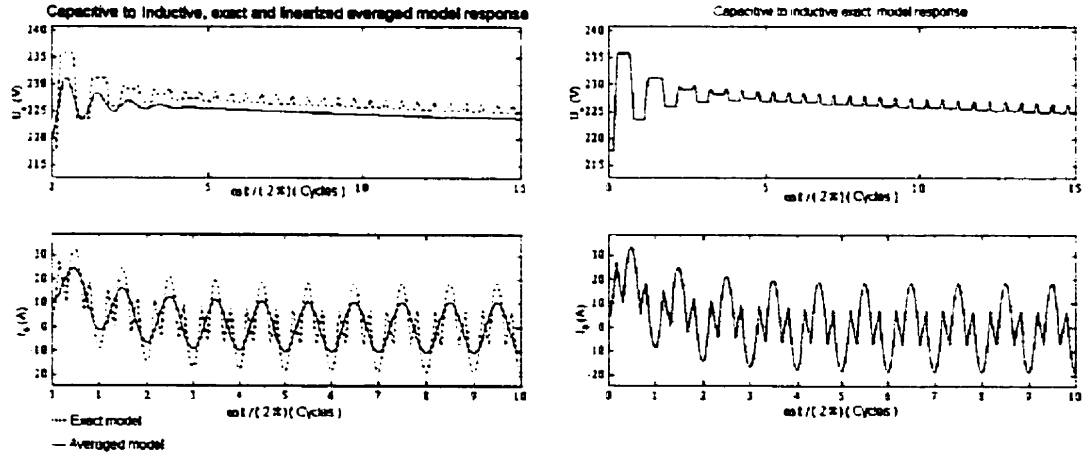

Figure 3.9. Dynamic responses of the compensator to a step change in current from 11.31 A peak inductive to 11.31 A peak capacitive, achieved with the average model (left) and the exact model (right).

3.3.4 Performance Measures

The performance of the compensator to a step change in current using the δ-μ feedforward control is depicted in Figure 3.10. A comparison between this figure and Figure 3.5 highlights the advantage of the δ-μ control over the δ control. Tables 3 and 4 summarize the performance of the compensator using the δ-μ feedforward control.

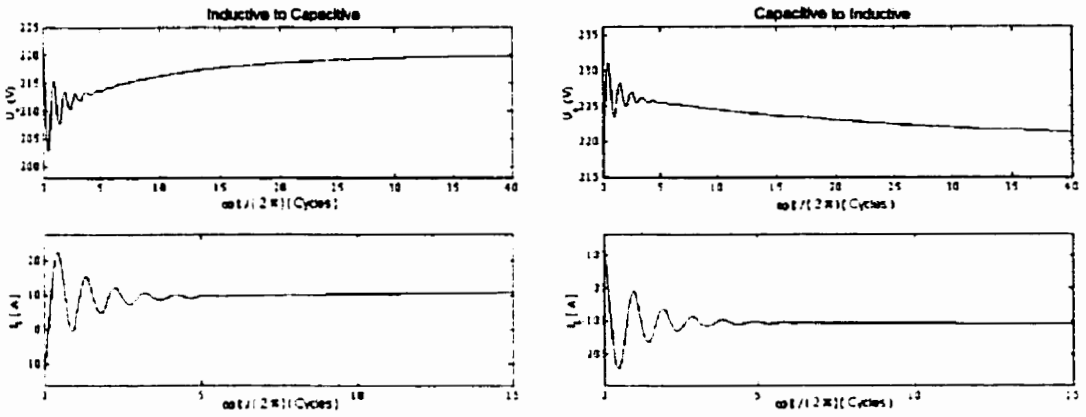

Figure 3.10. Step change in current from inductive to capacitive (left) and for capacitive to inductive (right) when the compensator uses the δ-μ feedforward control.

These tables show that the percent overshoot has a high value when the compensator changes its mode of compensation. This result has a significant impact on the power electronic switching elements, as they must be able to withstand this amount of current for a short period of time. Moreover, the rise time provides key information on the di/dt that the electronic device must be able to withstand. These tables also show that the over-voltage across the capacitor is no longer a concern. Comparisons between these two tables show that the percent overshoot is lower for a step change in current from inductive to capacitive, than vice-versa. This result indicates that, the system is more damped in capacitive mode.

Table 3.2 δ = - 2° to 2° and $\mu = f(\delta)$

VOLTAGE MEASURESS		CURRENT MEASURESS	
Percent over-voltage [%]	7.756976	Percent overshoot [%]	99.139231
Time to achieve the over-voltage [s]	0.007752	Time to peak [s]	0.007502
Settling time [s]	0.139035	Time to rise [s]	0.004251
Steady-state error [%]	0.009605	Settling time [s]	0.396349
		Steady-state error [%]	0.047300

Table 3.3 δ = 2° to - 2° and $\mu = f(\delta)$

VOLTAGE MEASURESS		CURRENT MEASURESS	
Percent over-voltage [%]	5.071162	Percent overshoot [%]	120.17049
Time to achieve the over-voltage [s]	0.008002	Time to peak [s]	0.007752
Settling time [s]	0.181295	Time to rise [s]	0.004010
Steady-state error [%]	0.281235	Settling time [s]	0.627407
		Steady-state error [%]	0.819052

3.4 Robustness Issues

3.4.1 Steady-State Error

The results of the previous section along with the ones obtained in [1] justify the necessity of the control parameter μ. According to Equation (2.17), the inclusion of this new control parameter permits the development of a unique correspondence between δ, μ and U_o. Thus, it is now possible to maintain the voltage U_o at a constant level. Nevertheless Equation (2.17) represents the average model; the exact model has no easy mathematical expression that relates directly the variables U_o, δ and μ. Therefore the consequences of applying Equation (2.17) to feedforward μ to the exact model will lead to steady-state error in the response of the system. Nevertheless, it will be seen later that this equation will play a key roll in developing an expression for the exact model without

resolving Equation (2.35). Figure 3.11 shows the consequences of using feedforward control on the exact model with the erroneous μ while operating in stationary conditions. It is important to note that the parameter μ only affects the voltage level and not the shape of the fundamental component of the current.

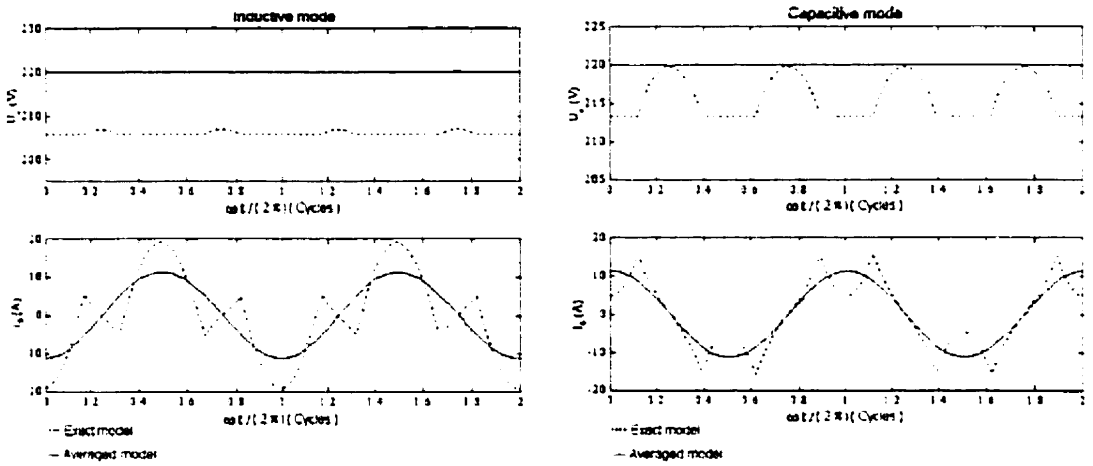

Figure 3.11. Stationary responses of the compensator in inductive and capacitive mode when the both models exact and average are feedforward with the same μ.

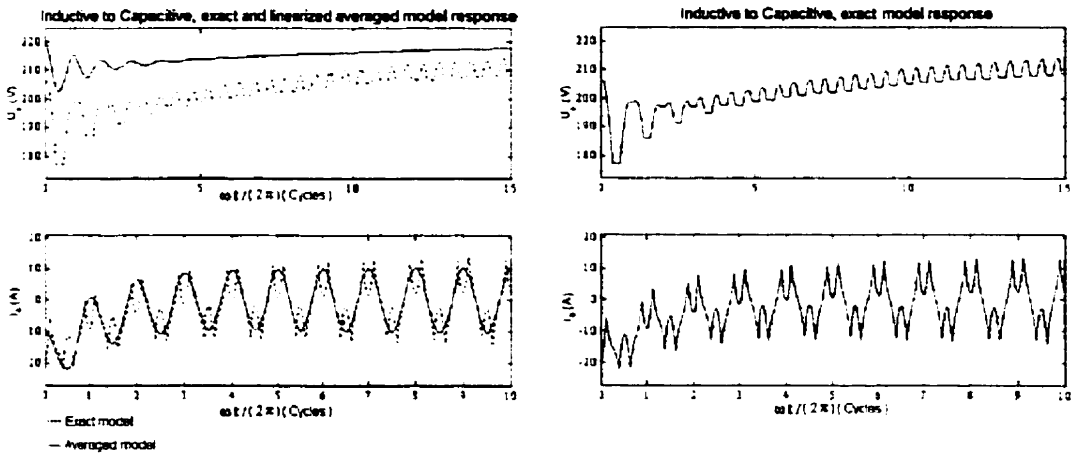

Figure 3.12. Dynamic responses of the compensator in inductive and capacitive mode when both models exact and average are feedforward with the same μ.

Figures 3.12 and 3.13 show the responses of the exact model under dynamic conditions when the compensator uses feedforward control with the wrong μ. Figure 3.12 shows the transient performance from inductive to capacitive mode, while Figure 3.13 shows the reverse change. Again it is important to note that the parameter μ only affects the voltage transient level and not the shape of the fundamental component of the current.

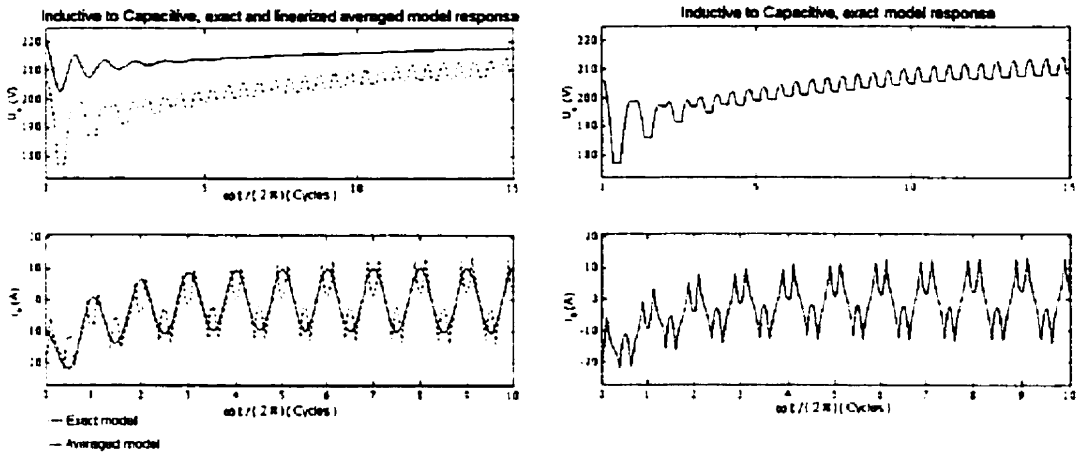

Figure 3.12. Dynamic response of the compensator from inductive to capacitive mode when both models are feedforwarded with the same μ.

3.4.2 Parameter Variation

In order to find an expression to calculate the value of μ for the exact model, Equation (2.35) was solved iteratively with the aid of a computer program, setting U_o constant and solving for μ while varying δ at increments of 0.2° within the interval from –5° to +5°. The recorded values of μ were later compared with the values given by Equation (2.17) and a seventh order polynomial was developed to calculate the amount of correction needed to adjust the values given by Equation (2.17). The 7-order polynomial has the following form:

$$\mu_a = 0.0001\delta^7 + 0.0005\delta^6 - 0.0019\delta^5 - 0.0081\delta^4 + 0.0342\delta^3 + 0.0326\delta^2 - 0.4345\delta + 3.4781 \quad (3.1)$$

Figure 3.14 shows the difference between the values obtained with Equation (2.17) and the values of μ obtained with Equation (2.35). It also shows the amount of correction achieved using the developed polynomial.

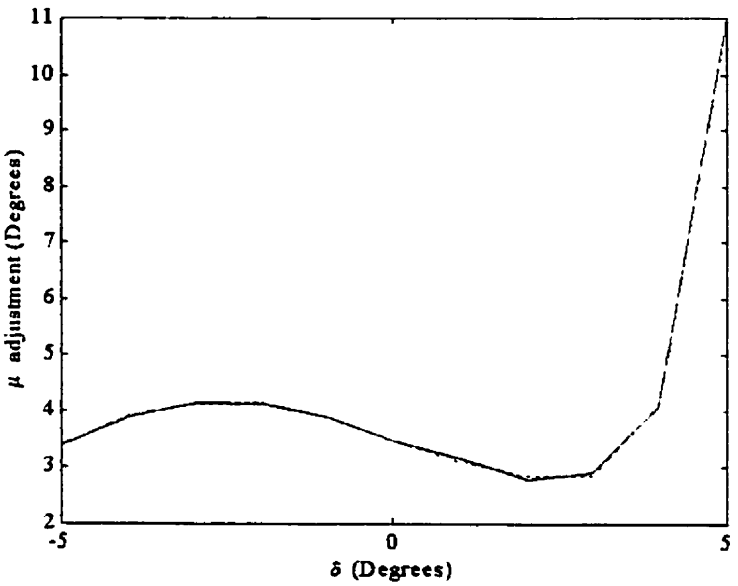

Figure 3.13. Amount of adjustment needed in Equation (2.15) to feedforward accurately the value of μ to the exact model.

CHAPTER 4

FEEDFORWARD / U_0 – FEEDBACK CONTROL

4.1 Motivation

This chapter is concerned with determining the optimal gain constant necessary for the implementation of a proportional control law. The implemented control law uses the voltage error to make the corrective action over the parameter of control, which might be δ or μ.

The influence of the negative feedback voltage-loop over the system's transient response is analyzed with the aid of two control strategies. One strategy uses δ as the parameter of control, while the other one uses μ. Following the previous work done by [1], whereby the parameter μ is fixed, a third control configuration, wherein δ is the controlled parameter and μ is held constant at 120° is also analyzed. The comparison between the latter strategy and the former configurations will yield observation about the advantage of having one more degree of freedom.

The control schemes of this chapter are based on the open-loop transfer functions given by Equations (2.24) and (2.25) in Chapter 2. The criterion to determine the optimal gain constant is set after performing a detailed root locus dynamical analysis of the system's open-loop transfer function. Each control configuration is implemented in both the exact and the average model. Finally, in order to benchmark the average model and to estimate the performance measures, each model is submitted to step changes in reactive current, from inductive to capacitive mode and vice-versa

4.2 Sampled and Average dc Voltage

The control structures defined in this chapter modify either the parameter of control, δ or μ. This parameter is altered to a more adequate value by an adjustment factor, which is determined by multiplying the optimal gain by the measured difference between the voltage reference and the voltage output U_o.

For the linearized averaged model, the voltage reference is not a concern since the mathematical modelling of the system gave an equation that relates the variables U_o, μ and δ. Therefore, the system's voltage reference can be predicted using Equation (2.17) developed in Chapter 2. On the other hand, the mathematical method used to describe the behaviour of the exact model did not give an expression that directly relates the variables U_o, δ and μ.

The implementation of the control law in the exact model yields an equation to calculate the reference voltage, but the value of this voltage depends on when the voltage signal is

sampled. A close look at the results in Figure 3.7 indicates that the best moment to sample the voltage U_o is at the zero crossing of the network voltage. During this period, the characteristic of the curve is flat and thus the chance of error is reduced. Figure 3.7 also shows that the voltage reference depends on the mode of operation of the compensator. In the figure, the value for the reference in inductive mode is 219.79 V, while the reference for the capacitive mode is 217.77 V.

Implementing a computer program to solve Equation (2.35) and to sample at the zero crossing of the network voltage permits calculation of the exact values of the reference voltages. These values are plotted and then an equation that matches this plot is found. Figure 4.1 shows that Equation (4.1) describes reasonably well the exact voltage reference values. It also shows that the maximum error when applying this equation is less than 0.6V.

$\delta < -4.3°$

$$U_{ref} = 220 - 5.8e^{(-2.2\delta + 5.3)}$$

$-4.3 <= \delta <= -2.3$

$$U_{ref} = 222.7 - 0.89e^{(-0.81\delta + 1)}$$

$\delta > -2.3$

$$U_{ref} = 220 - 0.88e^{(-0.5\delta)}$$

(4.1)

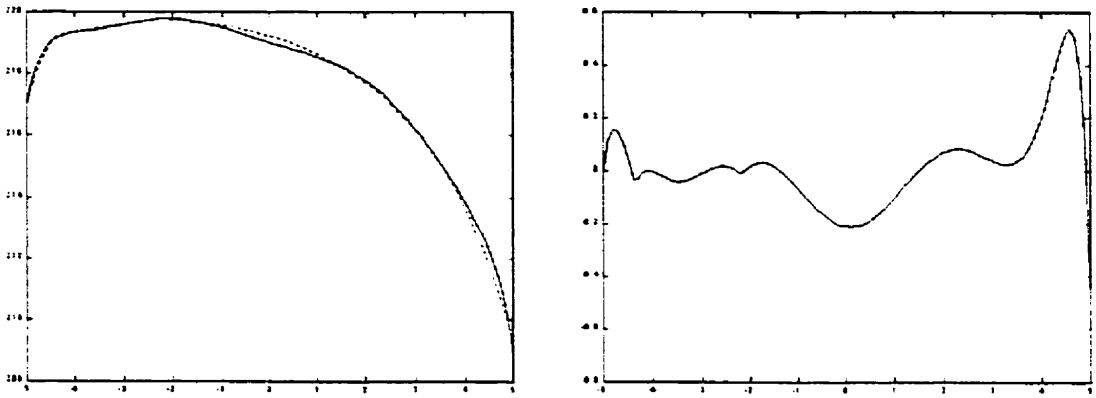

Figure 4.1. Exact reference voltage found by solving Equation (2.35) (solid left), reference voltage using Equation (4.1) (dotted left), and the amount of error when using the latter equation (right).

4.3 The δ - Feedforward / Uo – Feedback control with μ = 120°.

The mathematical analysis of the average model developed in chapter 2 describes a relationship between the variable U_o and the parameters of control δ and μ. This relationship can be used to determine the steady-state operating point of the compensator and the parameters of control. If μ is fixed to the value of 120° then expression (2.17) can be used to analyze the behaviour of the compensator as it was done by [1] and thus gain a deeper understanding of the results obtained and to outline the benefits of including the variable μ.

4.3.1 Control Structure

This control structure uses δ as the parameter of control with μ held constant at 120°. The configuration is depicted in Figure 4.2 and is composed of two diagrams. The upper one describes the control scheme to be implemented on the exact model, while the lower

one shows the control structure for the linearized average model, where the fixed value of μ is immersed in the open-loop transfer function G_μ.

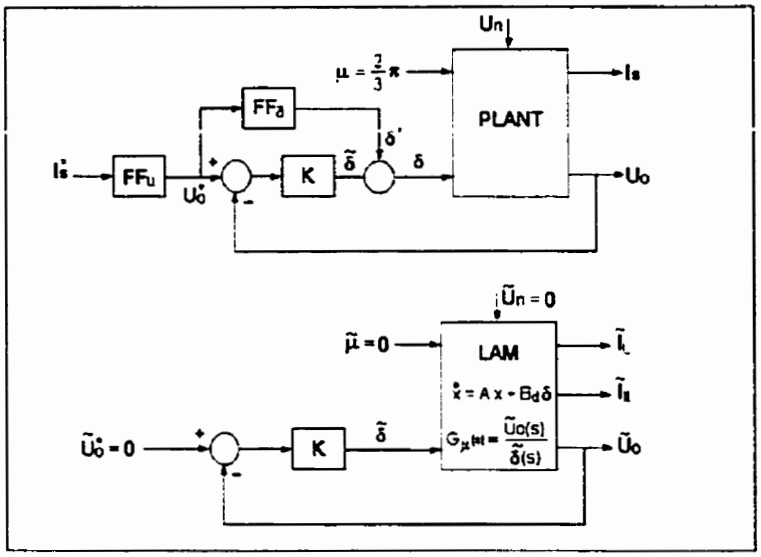

Figure 4.2. δ Feedforward / feedback control with μ=120° structure for the exact and the linearized average model.

The control law implemented in the exact model is easily seen by following the flow path of Figure 4.2. Expression (4.2) describes the control law for the exact model, while Equation (4.3) describes the control law implemented in the average model.

$$\delta=\delta^* + K(U_o^* - U_o) \tag{4.2}$$

$$\delta= - KU_o \tag{4.3}$$

Both configurations show a negative feedback voltage-loop. In steady state, the variation of δ is zero and the system reduces to the δ feedforward-loop control described in section 3.2. During the transient, δ is either increased or decreased depending on the transition of

the mode of operation. When a step change in current is made from inductive to capacitive according to the results of Section 3.2.3 the output voltage increases; but, the feedforward-loop adjusts U_o^* to the desired final value making $U_o^* > U_o$ and thus $K(U_o^* - U_o) > 0$ so $\delta(t) > \delta^*$, which means that the controller is increasing δ in order to increment the voltage and reach the desired set point U_o^*. On the other hand, when the converse change is made, the output voltage decreases; but, the feedforward-loop adjusts U_o^* to the desired final value, making $U_o^* < U_o$ and thus $K(U_o^* - U_o) < 0$ so $\delta(t) < \delta^*$, which means that the controller is decreasing δ, in order to decrease the voltage and reach the desired set value U_o^*. The reference voltage for this type of control is determined for the two models (i.e., exact and average) by Equation (2.17). This approach will introduce a small error for the exact model, but it will help to explain the results obtained by [1].

4.3.2 Root Locus Dynamical Analysis

The numerator of the transfer function G_μ determines the positions of the open-loop poles in the s-plane. Since the numerator of Equation (2.24), with μ fixed at 120° corresponds to the numerator of $G_\mu(s)$, it becomes clear that the allocation of the poles in the s-plane depends only on the variable δ. Figure 4.3 describe the position of the poles in the s-plane while δ varies within its operational range.

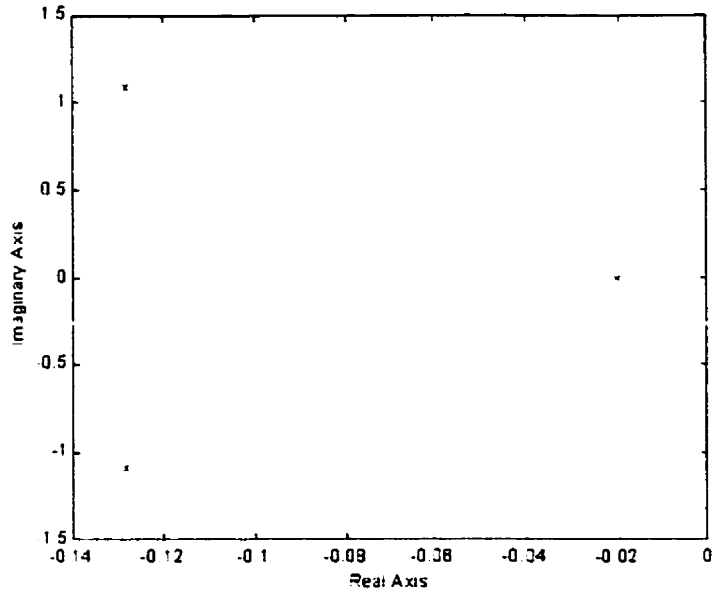

Figure 4.3. Open-loop poles of transfer function G_μ.

The denominator of Equation (2.24) with μ fixed at 120° corresponds to the denominator of G_μ which determines the position of the open-loop zeros. Figure 4.4 describes their dynamics as δ varies within its full range of operation.

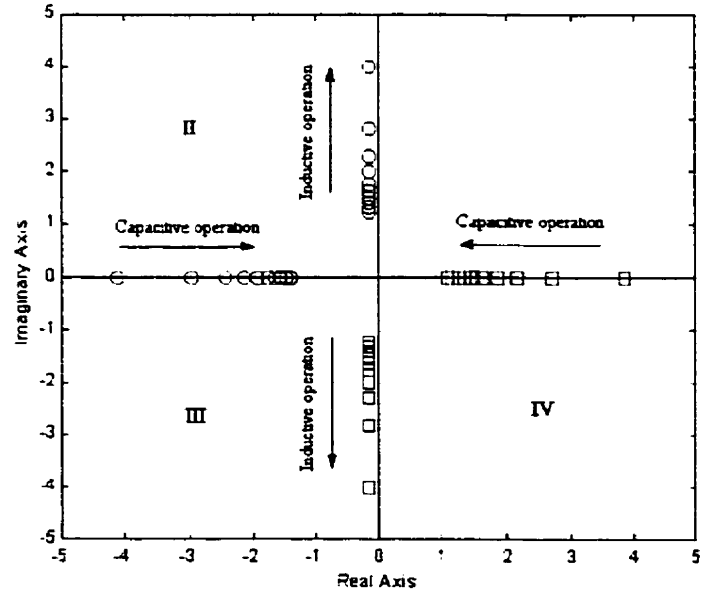

Figure 4.4. Open-loop zeros dynamics as δ and μ change over their interval of operation.

The open-loop complex zeros represented in Figure 4.4 describe the operation of the compensator in the inductive mode, while the real open-loop zeros depict the operation of the system in the capacitive mode. As the system advances from inductive mode toward the capacitive compensation mode, the imaginary part of the zeros increases until the neutral mode is reached. Therefore, the complex open-loop zeros located at the extremes (i.e., tail of the arrow) of quadrants II and III determine the operation of the compensator in its maximum inductive mode. The nearest real open-loop zeros to the origin determine the operation of the compensator in its maximum capacitive mode.

A close examination of Figures 4.3 and 4.4 permits the determination of the dynamics of the root locus. In inductive mode, as the gain increases, the upper complex closed-loop poles travel up right and then up left toward the complex open-loop zero. During this process, it is possible for the closed-loop poles just to touch or even to pass through the imaginary axis. The dynamics of the lower complex closed-loop poles are symmetrical to the poles just described. In the capacitive mode, the complex closed-loop poles will travel to the right, but this time they will meet each other at a point to the left of the real open-loop zero located over the positive side of the real axis. Beyond this point, both closed-poles will travel along the real axis but in the opposite direction -- one toward the open-loop zero and the other to plus infinity. Since the system is composed of three poles and two zeros, the root locus must have three branches, the above describing only two of them. The third branch starts at the real open-loop pole. The behaviour of this pole is independent of the mode of operation of the compensator. It always travels left; in the inductive mode, it goes to minus infinity, and in the capacitive mode, it ends at the

real open-loop zero located over the negative side of the real axis. Figure 4.5 depicts a typical root locus for the inductive and for the capacitive operation.

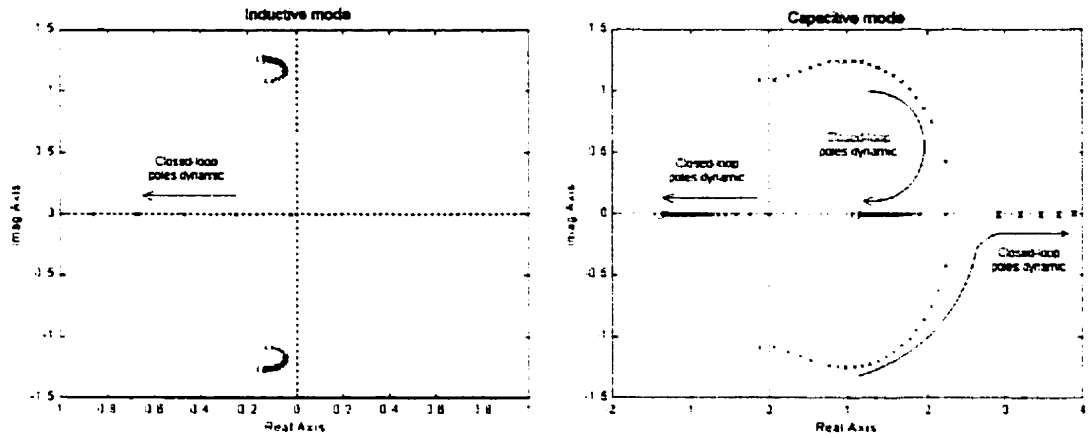

Figure 4.5. Typical root locus for inductive mode (left) and for capacitive mode (right).

4.3.3 Optimal Gain Determination

A simple analysis of Figure 4.5 shows that independent of the mode of operation, the initial movements of the complex closed-loop poles are to the right, while the dynamic of the real closed-loop poles is always to the left. Therefore, since they travel in opposite direction, the optimal gain is achieved when the real and the complex poles align because this will yield poles with about the same damping. Figure 4.6 depicts the values of the optimal gain as well as the maximum gain; this latter has been achieved when the complex closed-loop poles reach the imaginary axis. Notice that for values of δ<-4.3, the critical or maximum gain is infinity. Thus, for these values the system is always stable. The values for the optimal gain range between [0.0041 , 0.0025] rad/ V.

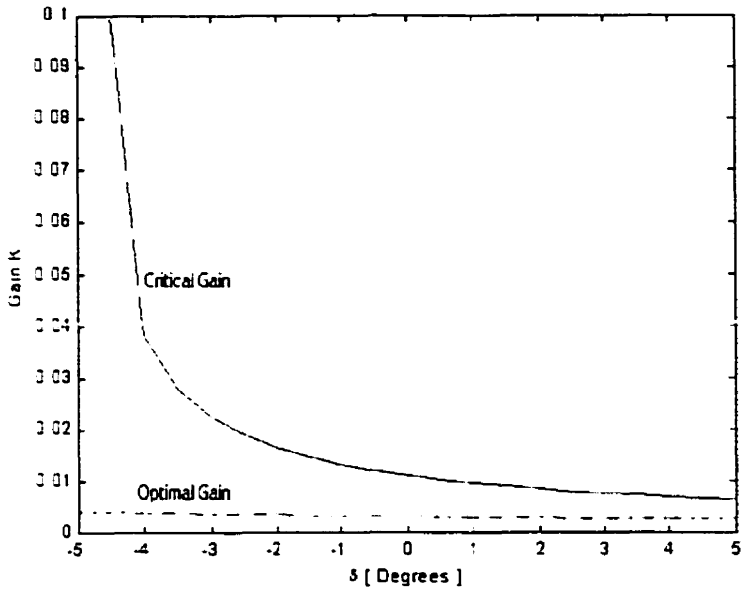

Figure 4.6. Critical gain (solid line) and optimal gain (dotted line).

The results obtained for the optimal gain guarantee the stability of the system; this means that the maximum of these values can be set as the gain of the system. The reason for choosing the maximum optimal gain as the gain of the system is based on the knowledge that high values of gain improve the performance of a feedback control system. Nevertheless, the consequences of setting just one value of gain for the whole range of operation of the compensator will come to light when submitting the system to step changes in reactive current. Figure 4.7 depicts the behaviour of one complex closed-loop pole when the system operates in its full range, using three different gains. It is important to observe how the closed-loop poles approach the imaginary axis, since this will permit a prediction of the behaviour of the compensator. The figure suggests a less damped oscillatory behaviour in capacitive mode.

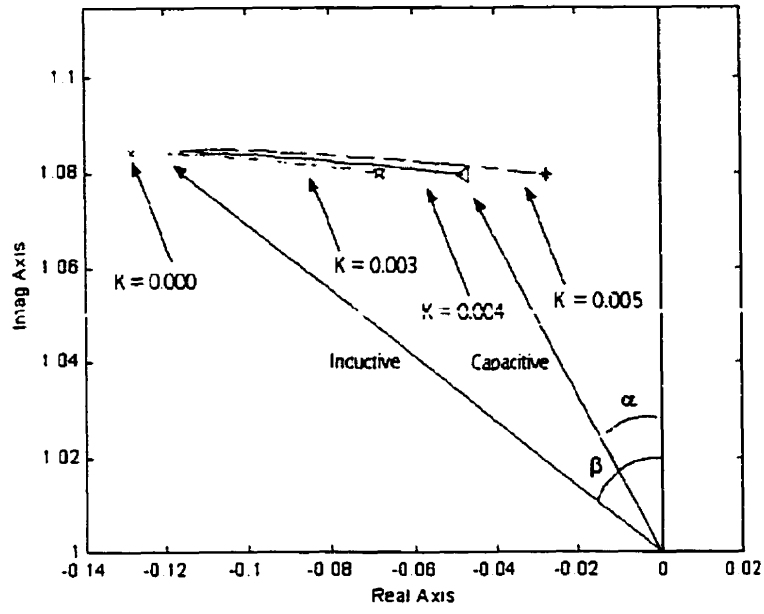

Figure 4.7. Dynamic of one complex closed-loop pole for three different gains.

According to the results of Figure 4.7, it can be seen that indeed k=0.004 gives the best option for the gain of the system. With the other two values, the system either gets too close to the unstable region or the gain is just too small. This figure, in conjunction with Figure 4.4, permits prediction of the behaviour of the compensator when the system is submitted to a step change in reactive current. When the system is working in inductive mode and is asked to change to capacitive mode, the transient oscillation will be higher in comparison with the converse change. This is due to the proximity of the closed-loop poles to the imaginary axis in capacitive mode. This fact also permits a prediction that the current settling time will be higher for the change from inductive to capacitive.

4.3.4 LAM Response

The response of the linearized average model, when submitted to a step change in current from 11.31A peak inductive, to 11.31A peak capacitive, is described on the left side of Figure 4.8; the opposite transition is depicted on the right side. Notice that the transient oscillation for the former change is higher than the transient oscillation for the latter one. Also, notice from the system's current comportment that the system is more damped in the inductive mode that in the capacitive mode.

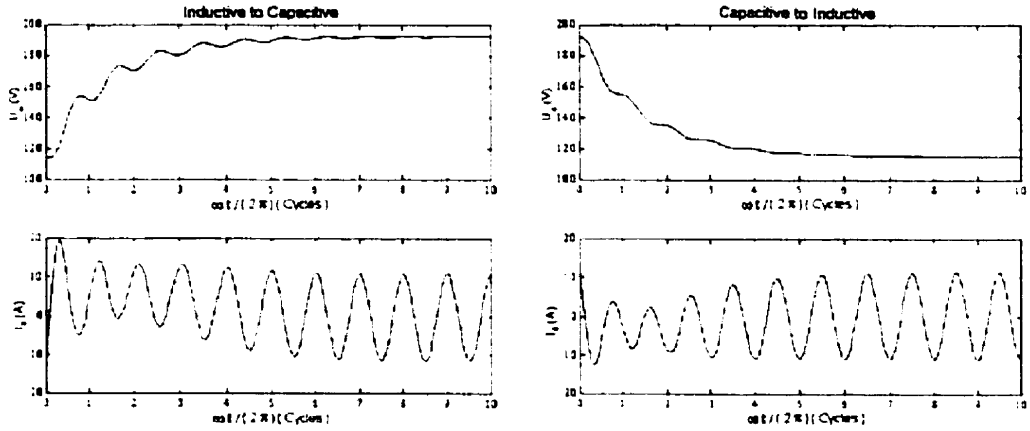

Figure 4.8. Linearized average model response for a step change from inductive to capacitive (left) and vice-versa (right).

4.3.5 Exact Response and Comparison With the LAM Response

The left side of Figure 4.9 shows the exact model response to a step change in current from 11.31A peak inductive to 11.31 A peak capacitive, while the converse transient is described on the right. The comparison between the two models is depicted in Figure 4.10.

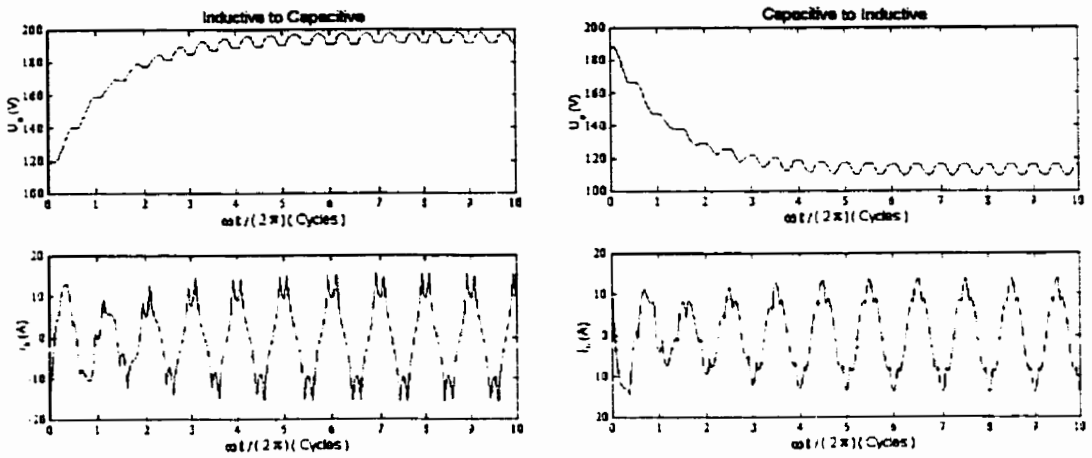

Figure 4.9. Exact model response for a step change from inductive to capacitive (left) and vice-versa (right).

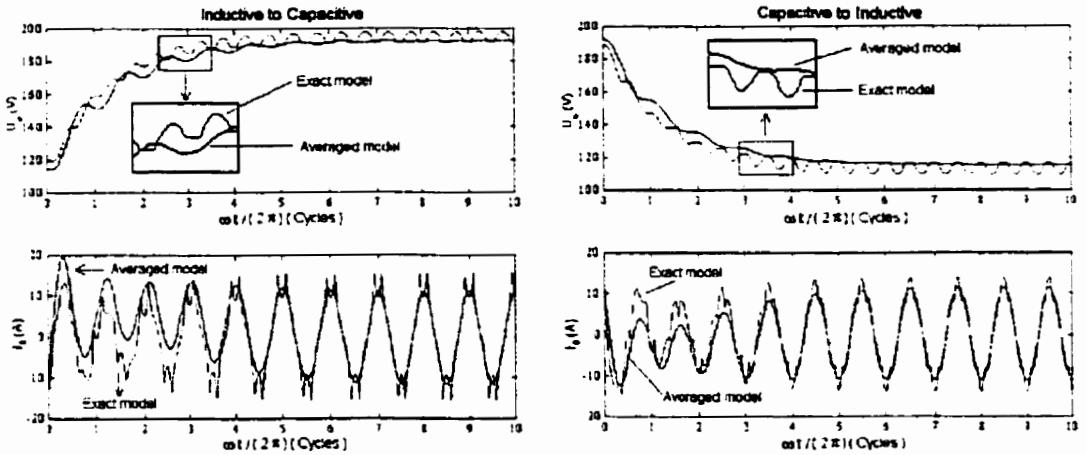

Figure 4.10. Comparison between the exact and the average model for step changes in reactive current from inductive to capacitive (left) and vice-versa (right).

The results in Figure 4.10 show that the average model represents reasonably well the exact model; but, moreover the exact model developed in Chapter 2 indeed behaves like the actual laboratory prototype developed by [1].

4.3.6 Performance Measures

The evolution of the reactive current during the transition from inductive to capacitive and vice-versa is depicted in Figure 4.11, which also shows the capacitor voltage transient. Notice that the reactive current oscillation during the transient is higher for the step change from inductive to capacitive. The evaluation indices associated with both step changes in reactive current are shown in Tables 4.1 and 4.2. The first table is concerned with the change from inductive to capacitive, while the second is associated with the change from capacitive to inductive. Both tables show the indices for the transient related to the voltage and to the current. Notice that the settling time and the oscillation are higher for the step change from inductive to capacitive in comparison with the opposite, as predicted.

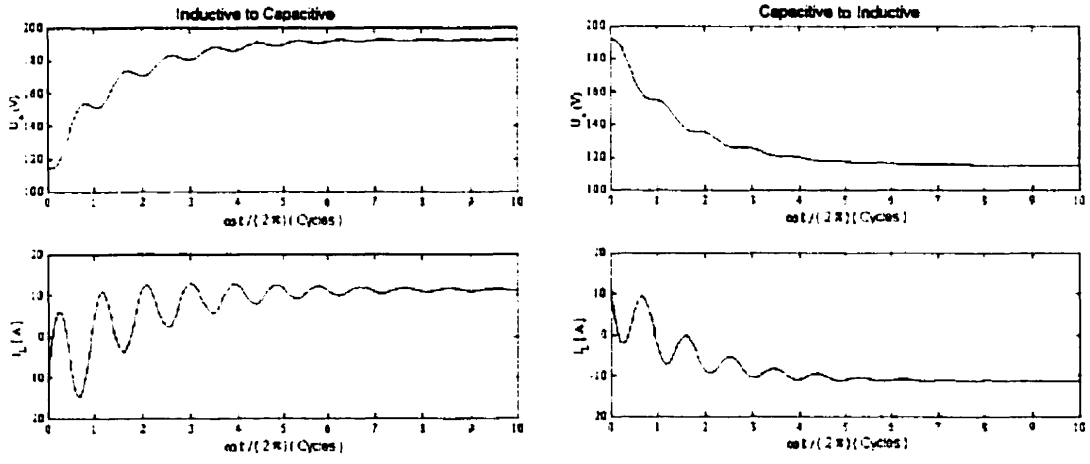

Figure 4.11. Step change in reactive current from inductive to capacitive (left) and from capacitive to inductive (right).

Table 4.1 $\delta = -2^{o}$ **to** 2^{o}

VOLTAGE MEASURES		CURRENT MEASURES	
Time to rise [s]	0.048549	Time to rise [s]	0.061562
Settling time [s]	0.069070	Settling time [s]	0.166166
Steady-state error [%]	5.1*10^-6	Steady-state error [%]	0.000118

Table 4.2 $\delta = 2^{o}$ **to** -2^{o}

VOLTAGE MEASURES		CURRENT MEASURES	
Time to rise [s]	0.049550	Time to rise [s]	0.048549
Settling time [s]	0.083083	Settling time [s]	0.120621
Steady-state error [%]	3. *10^-6	Steady-state error [%]	8.7*10^-8

4.4 The δ / μ Feedforward / U_o – Feedback to δ Control

This section is concerned with the performance analysis of the feedforward/feedback scheme using phase-shift/pulse-width control. The voltage feedback loop is used to modify the parameter of control δ.

4.4.1 Control Structure

The δ/μ feedforward / U_o – feedback to δ control is shown schematically in Figure 4.12 and is composed of two diagrams. The upper one depicts the control structure for the exact model and the lower one the control for the average model. The transfer function used by the average model corresponds to Equation (2.24) ($G_{31}(s)$)

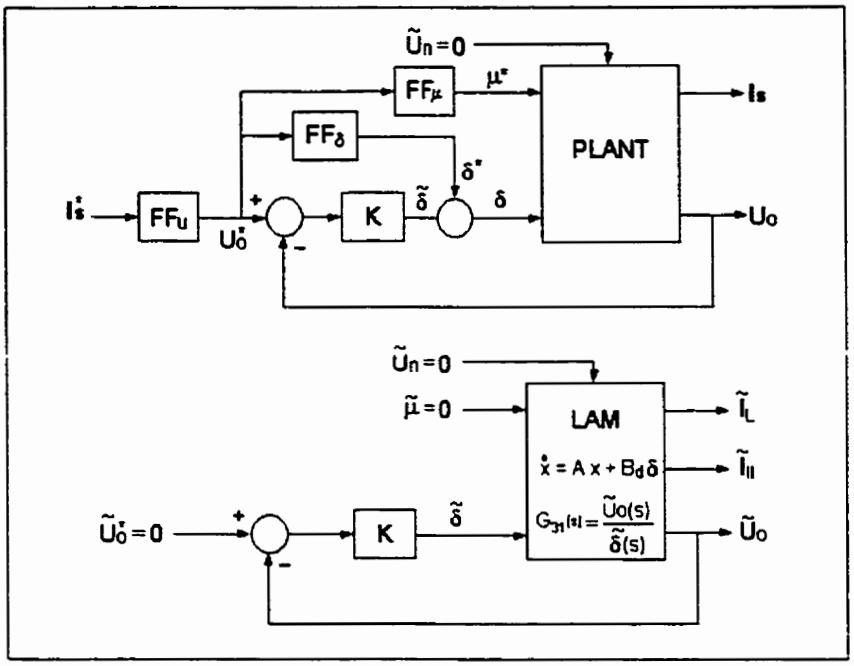

Figure 4.12. The δ / μ Feedforward / Uo – Feedback to δ Control, for the exact and for the linearized average model.

The control strategy for the exact model is composed of one feedforward loop for the parameter of control μ, and one negative feedback control loop used to proportionally modify the parameter of control δ, depending on the difference between the voltage set point and the output voltage. Equations (4.4) and (4.5) give the expressions for the control laws applied to the exact and the average model respectively.

$$\delta=\delta^{*} + K(U_o^{*} - U_o) \tag{4.4}$$

$$\delta= - KU_o \tag{4.5}$$

Notice that these equations differ from Equations (4.2) and (4.3), just by the value of K. However, the open loop transfer functions are totally different. In steady state, the derivative of δ with respect to time is zero and the system reduces to the δ-μ feedforward control on section 3.3. In this scheme, the voltage reference is calculated differently for each model. While Equation (2.17) gives the voltage reference for the average model, Equation 4.1 calculates the voltage reference for the exact model.

4.4.2 Root Locus Dynamical Analysis

The position of the system's open-loop poles and zeros are determined respectively by the denominator and the numerator of the feedforward transfer function $G_{31}(s)$. In this expression, both the numerator and denominator are functions of the parameters δ and μ. Therefore, the dynamics of the open-loop zeros and open-loop poles depend on the values of δ and μ. Figure 4.13 shows the movements of the open-loop poles while the parameters of control vary within its full range of operation.

The points marked with an "x" in Figure 4.13 denote the position of the open-loop poles when the compensator is working in its maximum inductive mode. The figure also shows that as the compensator moves from inductive to capacitive mode, the complex open-loop poles move closer to the imaginary axis, while the real open-loop pole moves away from this axis.

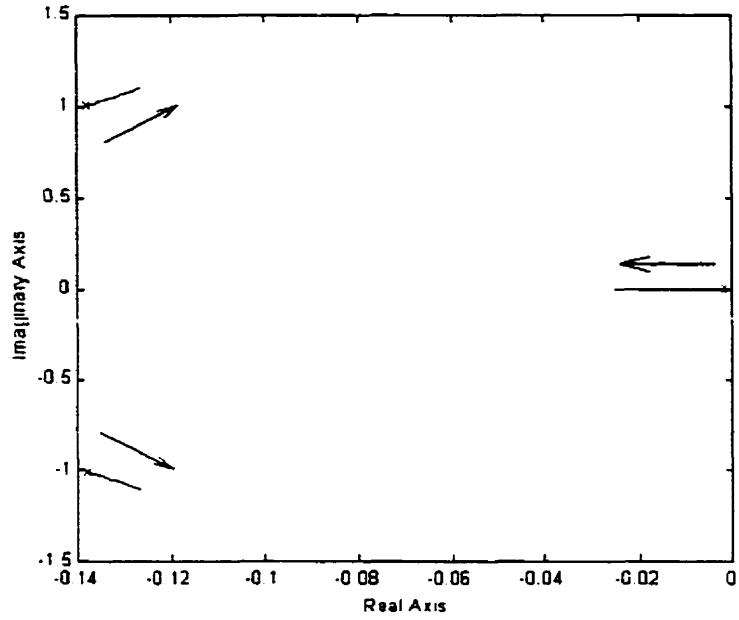

Figure 4.13. Dynamics of open-loop poles

The movement of the open-loop zeros is depicted in Figure 4.14. As expected, the dynamic is very similar to the previous control structure. Again, when the system works in the inductive mode, the open-loop zeros are formed by a real and an imaginary part; the latter increases as δ increases. When the systems work in capacitive mode, the open-loop zeros are real and they approach the imaginary axis as δ increases.

The dynamics of the root locus can be broadly determined with the aid of Figures 4.13 and 4.14. When the compensator is working in the inductive mode, the complex closed-loop poles of Figure 4.13 travel toward the complex open-loop zeros of Figure 4.14. The trajectory of this path may or may not cut the imaginary axis, depending on the start point of the root locus. In the capacitive mode, the complex closed-loop poles travel right, to meet each other at a point to the right of the positive real open-loop zero. Beyond this

point, one pole travels to plus infinity along the real axis, while the other travels toward the real open-loop zero.

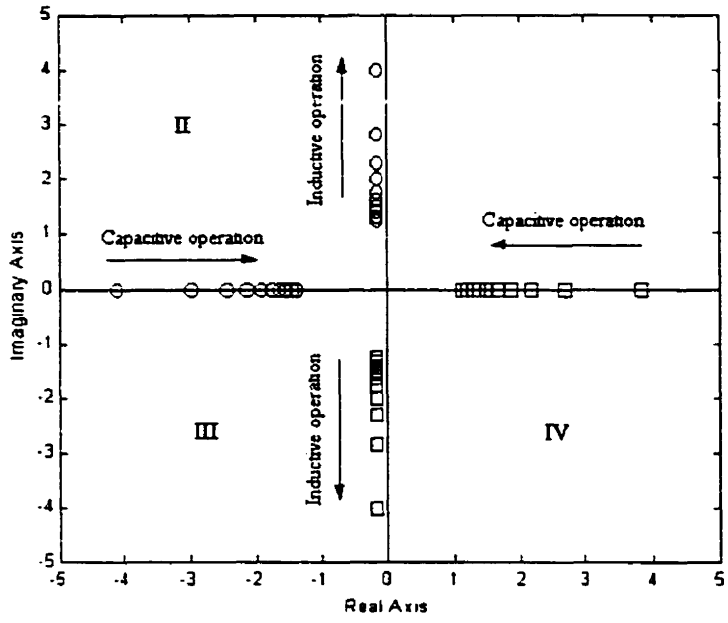

Figure 4.14. Dynamics of the open-loop poles for the feedforward transfer function the δ / μ Feedforward / U_o – Feedback to δ Control structure.

The above describes two of the three branches of the root locus; the third is composed by the closed-loop poles that start at a real open-loop pole on Figure 4.13. The movement of these poles is always to the left, independent of the compensation's mode. However, the distance traveled by these poles between two equal consecutive increments in gain is different. In the inductive mode, the steps are larger than in the capacitive mode because in the former mode, the poles must travel to minus infinity, while in the capacitive mode there is always an open-loop zero over the negative real axis, which determines the end point of the branch of the root locus.

The comportment of these closed-loop poles will have a significant impact on the value of the optimal gain. Figure 4.15 describes a typical root locus for the compensator operating in the inductive mode as well as a typical root locus when the compensator is operating in the capacitive mode.

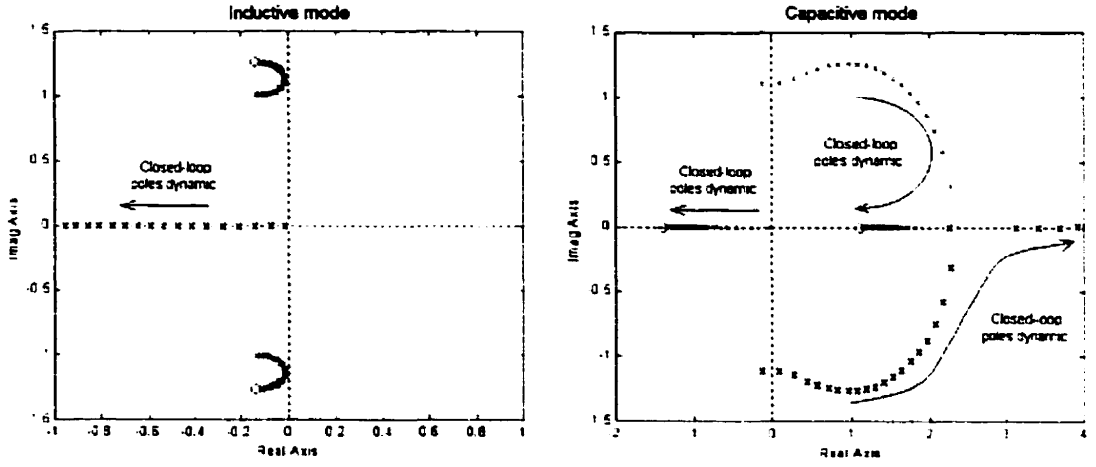

Figure 4.15. Typical root locus for inductive mode (left) and for capacitive mode (right).

4.4.3 Optimal Gain Determination

A simple analysis of Figure 4.15 shows that independent of the mode of operation, the initial movements of the complex closed-loop poles are to the right, while the dynamic of the real closed-loop poles is always to the left. Therefore, since they travel in opposite directions, the optimal gain is achieved when the real and the complex poles align. Figure 4.16 depicts the values of the optimal gain as well as for the maximum gain; this latter has been achieved when the complex closed-loop poles reach the imaginary axis. Notice that for values of δ<-4.3, the critical or maximum gain is infinity. Thus, for these values the system is always stable. The values for the optimal gain range between [0.018

, 0.0025] rad/ V. Notice that for the majority of the inductive range the optimal gains are higher than the maximum (or critical) gain in the capacitive mode; therefore, the system's gain will be limited by the maximum gain.

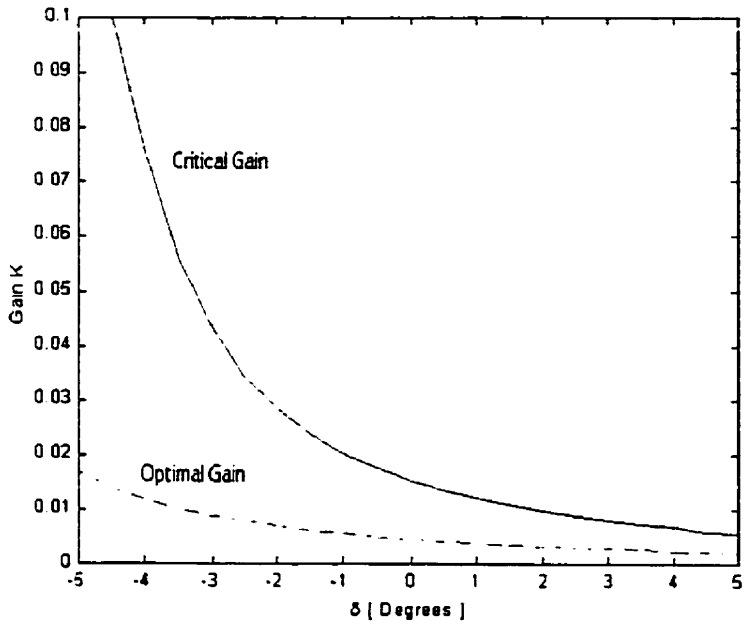

Figure 4.16. Critical gain (solid line) and optimal gain (dotted), for the compensator over its operating range.

Since not all the results obtained for the optimal gain guarantee the stability of the system over its full operating range, the minimum critical gain is used as the optimal gain of the system. Figure 4.17 shows the dynamics of one complex closed-loop pole when the system operates over its full operating range using three different gains: 0.004, 0.005 (the optimal gain for the system) and 0.006 [rad/V].

The results described by Figure 4.16 illustrates that the value 0.005 is the highest possible value of the gain for the system in order to remain stable over its full operating range.

Notice that Figure 4.17 shows that there are operating points in the capacitive mode where the system becomes unstable with a gain value of 0.006 [rad/V]. From this figure, in conjunction with Figure 4.13, it is possible to predict that the system will be more damped and have less transient oscillation when the compensator moves from capacitive to inductive in comparison with the opposite change. This finding again is due to the proximity of the closed-loop poles to the imaginary axis when the compensator works in the capacitive mode. Since in both modes of operation the dominant closed-loop poles are very near to the imaginary axis, high values of percent overshoot are expected.

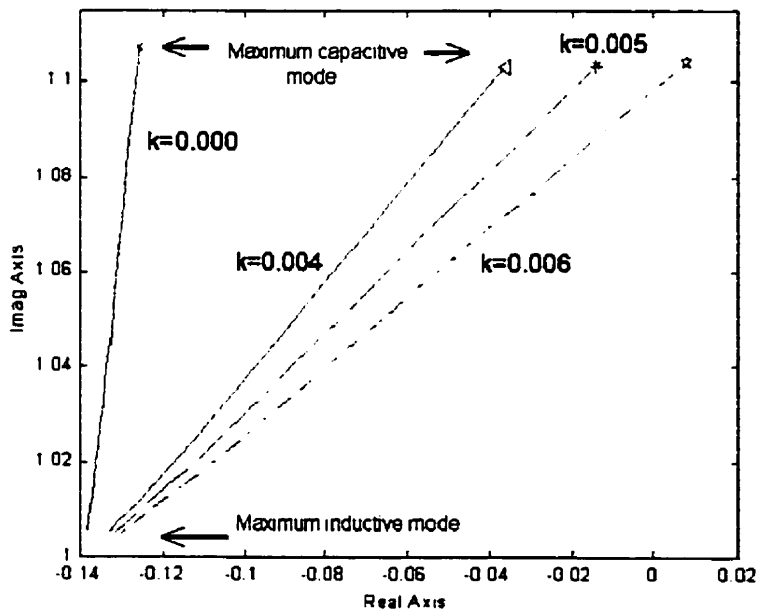

Figure 4.17. Dynamic of one complex closed-loop pole when the system uses three different gains.

4.4.4 LAM Response

The results depicted in Figure 4.18 confirm the predicted behaviour of the compensator. As can be seen, a step change in reactive current from inductive to capacitive produces a voltage output less damped and with more transient oscillation than a step change in reactive current from capacitive to inductive. This result also applies to the dynamic behaviour of the reactive current, as will be seen in latter results. The figure describes the behaviour of the voltage and the system's current when submitted to a step change in reactive current from 11.311A peak inductive to 11.311A peak capacitive, and vice-versa. Notice that the voltage variation is far less with this control structure than with the δ - Feedforward / U_o – Feedback control with μ = 120°.

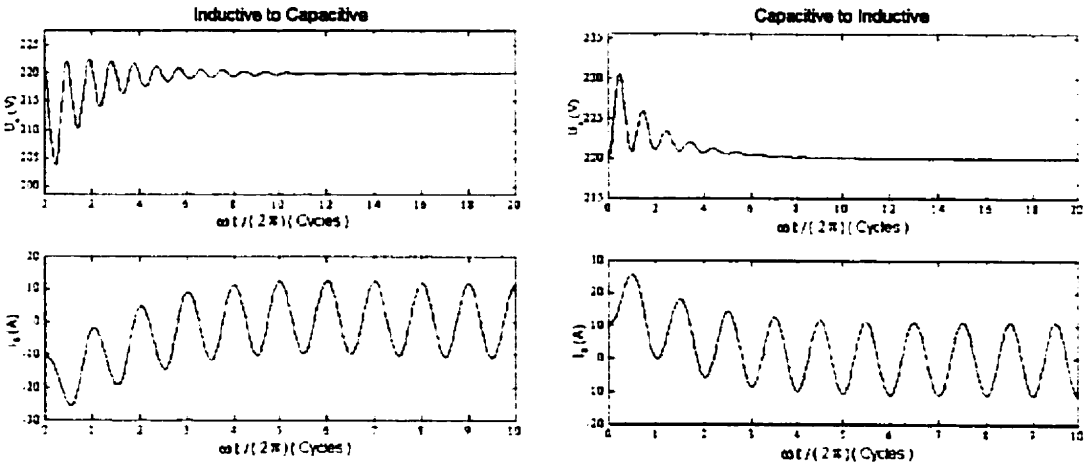

Figure 4.18. Linearized average model response for a step change from inductive to capacitive (left) and vice-versa (right).

4.4.5 Exact Response and Comparison with the LAM Response

The exact responses of the compensator to the same step change in reactive current are depicted in Figure 4.19. The comparison between the exact and the averaged model for the same step changes are described in Figure 4.20.

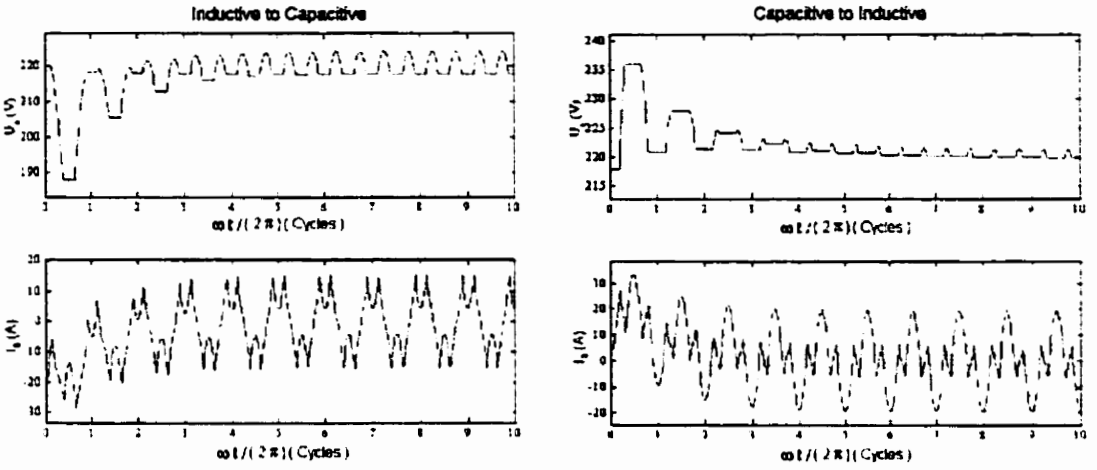

Figure 4.19. Exact model response for a step change in reactive current from inductive to capacitive (left) and from capacitive to inductive (right).

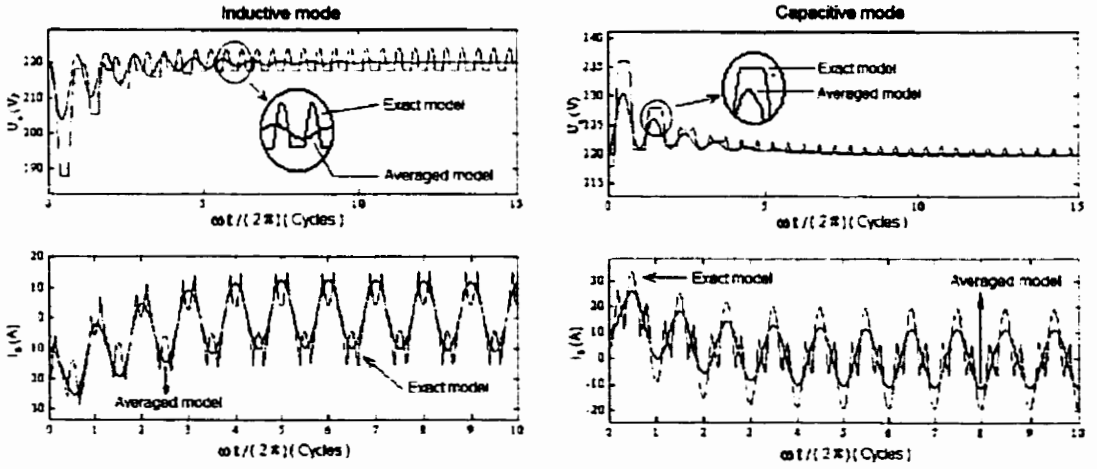

Figure 4.20. Comparison between the exact and the average model for a step change in reactive current from inductive to capacitive (left) and vice-versa.

4.4.6 Performance measures.

The evolution of the voltage and the reactive current during the transition from inductive to capacitive and vice-versa is depicted in Figure 4.21. These results ratify the predicted behaviour in voltage and reactive current when the system changes from one state to another. Notice that during the transient from capacitive to inductive mode, the system is more damped and it has also less oscillation than the converse transition. Therefore, the current settling time is smaller for the transient from capacitive to inductive in comparison with the opposite transient.

Notice also that the transient from capacitive to inductive gives the higher percent overshoot. This effect is due to the influence of the open-loop zeros. The closer the open-loop zeros are to the imaginary axis, the higher the percent overshoot. Figure 4.14 shows that in the inductive mode, the real part of the complex open-loop zeros is closer to the origin than the open-loop zeros in the capacitive mode.

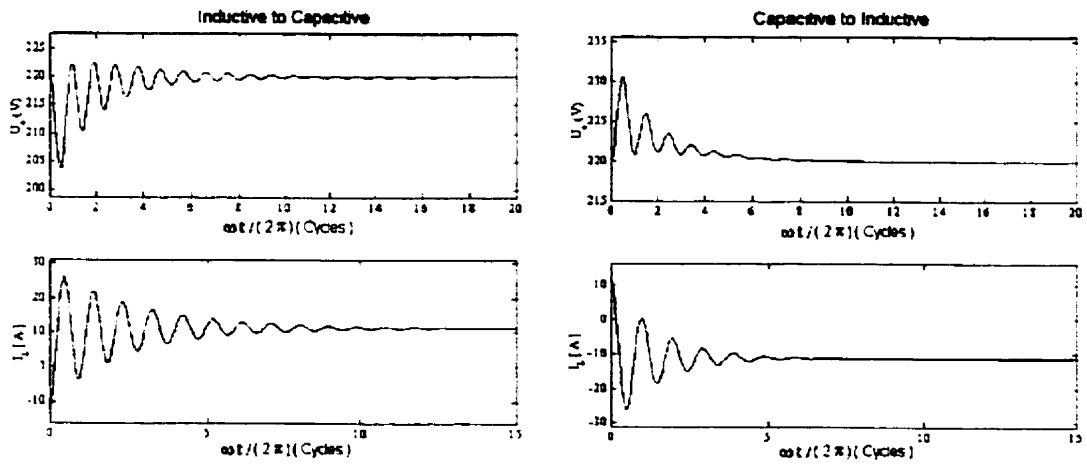

Figure 4.21. Voltage and reactive current evolution when the system is submitted to a step change in reactive current from inductive to capacitive (left) and vice-versa (right).

Table 4.3 δ = - 2° to 2°

VOLTAGE MEASURES		CURRENT MEASURES	
Percent over-voltage [%]	7.447547	Percent overshoot [%]	129.641124
Time to achieve the over-voltage [s]	0.007418	Time to peak [s]	0.007585
Settling time [s]	0.041177	Time to rise [s]	0.0040010
Steady-state error [%]	5.4*10^-5	Settling time [s]	0.18854
		Steady-state error [%]	0.001651

Table 4.4 δ = 2° to - 2°

VOLTAGE MEASURES		CURRENT MEASURES	
Percent over-voltage [%]	4.770545	Percent overshoot [%]	131.137337
Time to achieve the over-voltage [s]	0.007668	Time to peak [s]	0.007835
Settling time [s]	0.027090	Time to rise [s]	0.004084
Steady-state error [%]	0.000268	Settling time [s]	0.100358
		Steady-state error [%]	0.0005329

4.5 The δ / μ Feedforward / Uo – Feedback to μ Control

4.5.1 Control Structure

This control structure uses μ as the parameter of control. The configuration is depicted in Figure 4.22 and is composed of two schemes-- one for the exact model and the other for the linearized average model. The upper scheme describes the control structure for the exact model. The control law given in Equation (4.6) uses the error in the voltage to modify the parameter μ and is implemented in the exact model.

$$\mu = \mu^* - k(U_0^* - U_0) \tag{4.6}$$

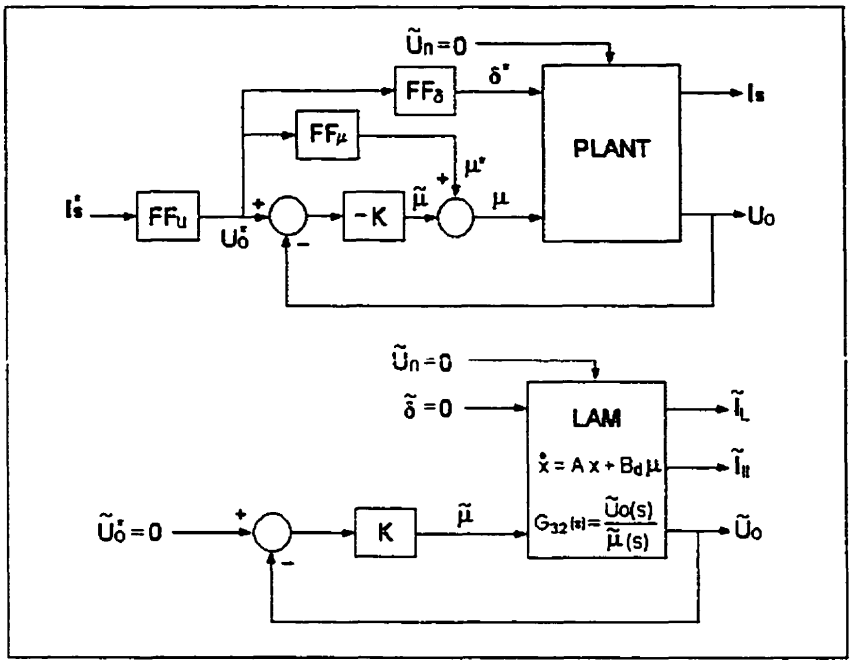

Figure 4.22. The δ / μ Feedforward / U_o – Feedback to δ Control, for the exact and for the linearized average model.

The lower scheme depicts the control structure implemented in the linearized average model. Equation (4.7) describes the control law applied in this model. The transfer function used by the average corresponds to Equation (2.25) ($G_{32}(s)$). Notice that the system is also described by its state space equation. Here $\mathbf{B_d}$ is the second column vector of the Jacobian matrix **B.**

$$\mu = - KU_o \tag{4.7}$$

4.5.2 Root Locus Dynamical Analysis

The dynamics of the open-loop poles are exactly the same as those depicted by Figure 4.13. On the other hand, the dynamics of the open-loop zeros are totally different.

Figure 4.23 describes how the open-loop zeros move along the s-plane as the parameters of control δ and μ vary within all their operational values.

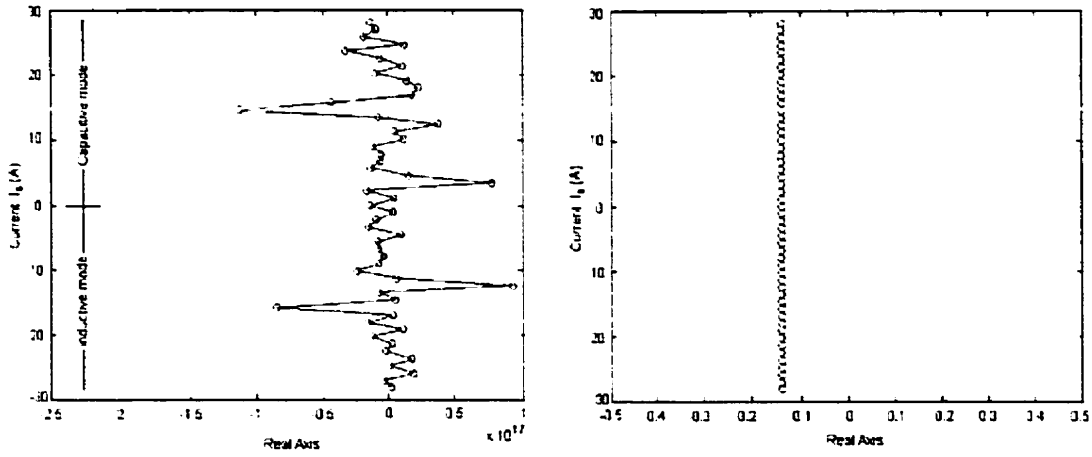

Figure 4.23. Zero dynamics of the compensator as the parameters δ and μ vary within all their operational values.

The results on Figure 4.23 show an oscillatory behaviour on both open-loop zeros. In the figure, the projection of the zero over the vertical axis gives the mode of operation of the compensator while the projection over the horizontal axis determines the actual position of the open-loop zero over the real axis of the s-plane. The amount of oscillation is significantly different for both zeros and it has no obvious correlation with the mode of operation of the compensator. Therefore, it is not possible to determine a rough sketch of the compensator when working in either mode of operation. Nevertheless a close look at Figure 4.23 in conjunction with Figure 4.13 indicates two distinct forms of the root locus.

It can be seen from Figure 4.23 that either the two open-loop zeros lay in the negative real axis or each one allocates in different sides of the real axis. In either case, there is always one zero on the s-plane very near to the origin in the negative side of the real axis.

Therefore, if the open-loop zeros lay on opposite sides of the real axis, the real open-loop pole and the positive real open-loop zero form one branch of the root locus. The Complex closed-loop poles and the remaining zeros form the other two branches. These branches have the starting point at the complex open-loop poles and as the gain increases, the complex closed-loop poles travel to the left in the s-plane and meet each other at a point to the left of the negative, real open-loop zero. At the point of encounter, the closed-loop poles travel in opposite directions; one travels right toward the zero and the other to minus infinity.

When both open-loop zeros lay in the negative side of the real axis, it is expected that the real open-loop pole and the open-loop zero nearest to the origin form one branch of the root locus. However, since in this case it is always possible to factorize a negative sign in the feedforward transfer function, the rules to sketch the root locus for a negative feedback system do not hold; therefore, the rules for a positive feedback loop must be applied. This fact suggest that one branch of the root locus formed by a closed-loop pole that travels to plus infinity with a start point at the real, negative open-loop pole. The other two branches are exactly the same as the ones described when the two zeros lay on different sides of the s-plane's real axis; the only difference in this case is that one pole will travel toward a zero, instead of minus infinity. Figure 4.24 depicts these two situations; the lower graphs describe the sketch of the root locus for very small gains ($k<0.05$)

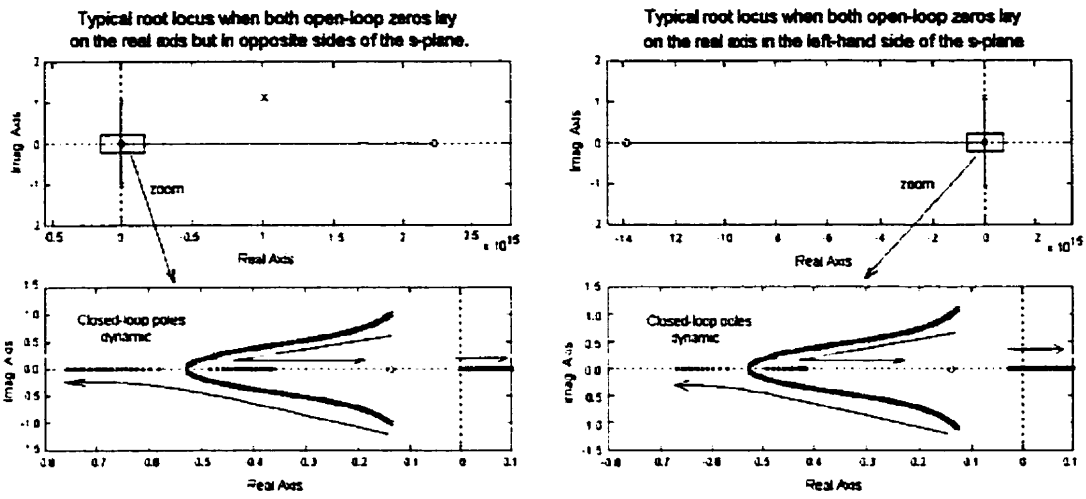

Figure 4.24 Typical root locus of the compensator when δ and μ vary within all their operational values.

4.5.3 Optimal Gain Determination

An interesting result that immediately comes to light from Figure 4.24 is the movement of some closed-loop poles toward the positive side of the s-plane regardless of the mode of operation; this comportment allows an immediate determination of the situation for the smallest critical gain. As can be seen from Figure 4.13, when the compensator is working in its most inductive mode, the real open-loop pole achieves the nearest position to the origin. Thus, this situation allows finding the lowest critical gain. Figure 4.25 show the values of the critical gain according to the values of δ and μ.

Since the minimum critical gain imposes the stability limit, the value of the optimal gain arises immediately. From Figure 4.25 the value for the system's optimal gain is 0.002 rad/V. This is a very low value for the gain and therefore the location of the closed-loop poles of the system will not differ significantly from the location of the open-loop poles.

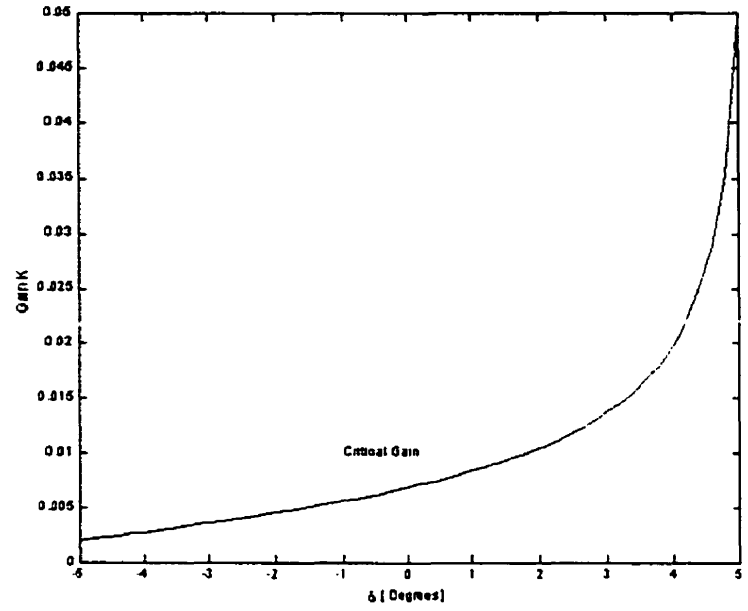

Figure 4.25 Critical gain according to the values of δ and μ.

Figure 4.26 show the movement of one complex closed-loop pole and the dynamics of the real closed loop pole when the gain is set to 0.002 rad/V. This figure also permits a prediction of the general behaviour of the compensator when submitted to a step change. Due to the proximity to the origin of all closed-loop poles a relatively large time constant is expected; therefore, slow decreasing or increasing exponential will characterize the feature of the responses. The settling time will be higher from inductive to capacitive than for the converse change; this is due to the higher time constants on the former mode of operation than in the latter.

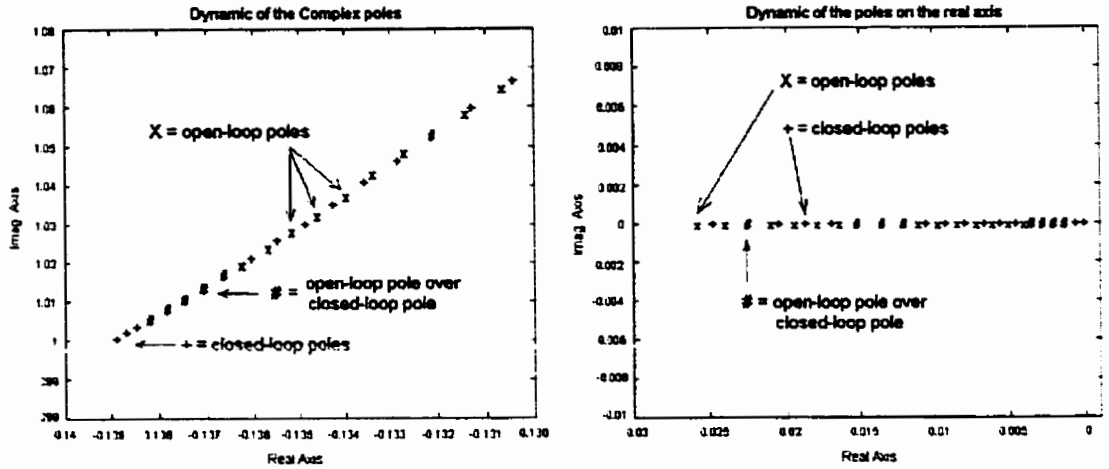

Figure 4.26. Closed-loop poles dynamics for a constant gain of 0.002 rad/V.

4.5.4 LAM Response

The response of the linearized average model when submitted to a step change in current from 11.31A peak inductive, to 11.31A peak capacitive, is described in the left side of Figure 4.27; the opposite transition is depicted in the right side. The results in this figure ratify the previous analysis of the compensator when submitted to a step change. It can be seen that in both changes, the system has a slow response; moreover, the response to a step change from capacitive to inductive is slower that the opposite change. This is due to the proximity of the closed-loop real pole to the origin in the inductive mode. The initial high oscillation is due to the proximity to the imaginary axis of the complex closed-loop poles.

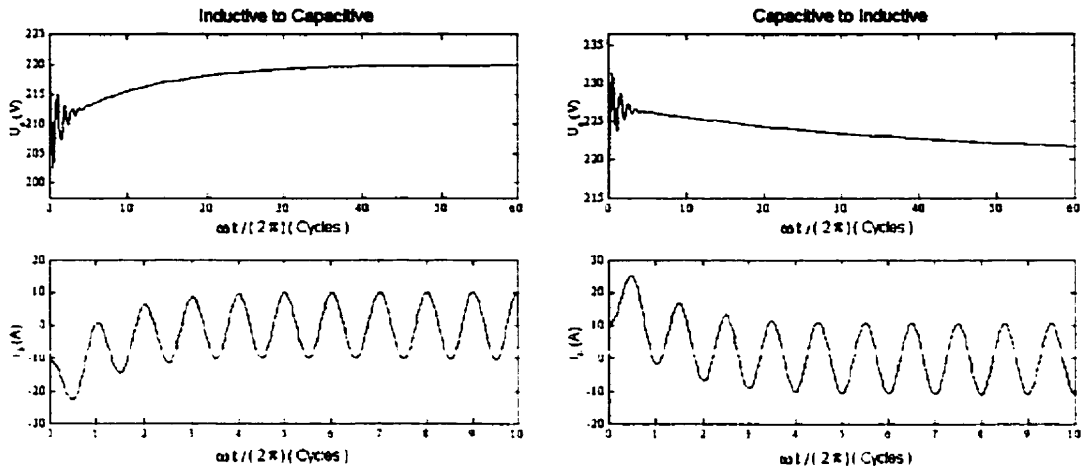

Figure 4.27. Linearized average model response for a step change from inductive to capacitive (left) and vice-versa.

4.5.5 Exact Response

The response of the exact model when submitted to a step change in current from 11.31A peak inductive, to 11.31A peak capacitive, is described in the left side of Figure 4.27; the opposite transition is depicted in the right side. The results in this figure ratify the previous analysis of the compensator when submitted to a step change. It can be seen that in both changes, the system has a slow response. Moreover, the response to a step change from capacitive to inductive is slower that the converse change. A more interesting result is the noticeable higher oscillation for a step change from inductive to capacitive mode than for the converse change; this result again is due to the relative proximity of the complex closed-loop poles to the imaginary axis. Figure 4.27 shows the comparison between the two models

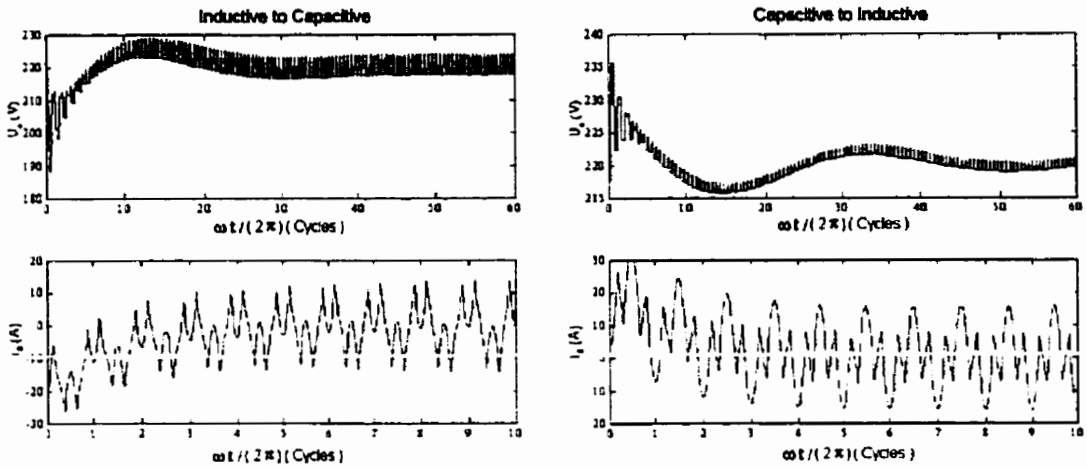

Figure 4.28. Exact model response for a step change from inductive to capacitive (left) and vice-versa.

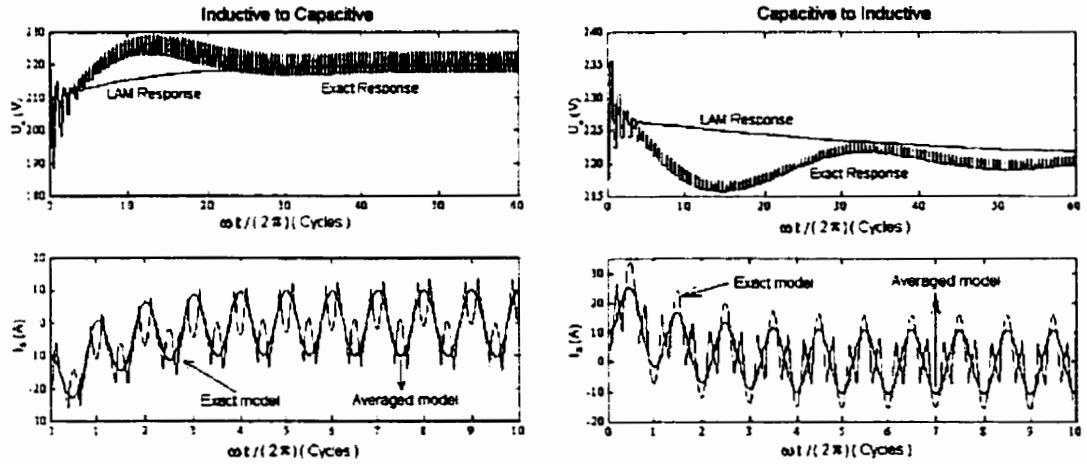

Figure 4.29. Comparison between the exact and the average model for step change in reactive current from inductive to capacitive (left) and vice-versa (right).

4.5.6 Performance Measures

The evolution of the voltage and the reactive current during the transient from inductive to capacitive and vice-versa is depicted in Figure 4.30. These results ratify the predicted behaviour in voltage and reactive current when the system changes from one state to

another. Notice that during the transient from capacitive to inductive mode, the system is slower and it has also more oscillation than for the opposite transient.

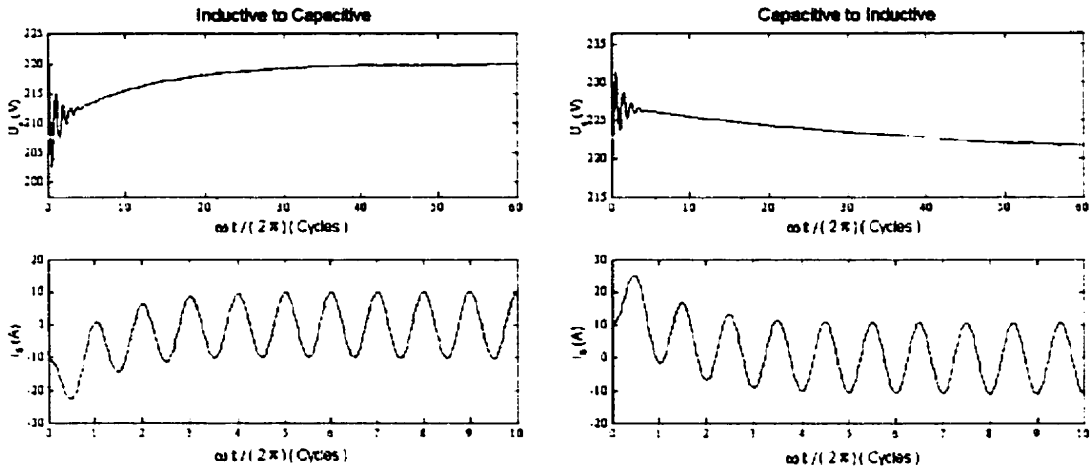

Figure 4.30. Step Change in reactive current from inductive to capacitive and vice-versa.

Table 5.1 δ = - 2° to 2°

VOLTAGE MEASURES		CURRENT MEASURES	
Percent over-voltage [%]	7.9340	Percent overshoot [%]	104.658268
Time to achieve the over-voltage [s]	0.008002	Time to peak [s]	0.007502
Settling time [s]	0.172293	Time to rise [s]	0.0040010
Steady-state error [%]	0.028417	Settling time [s]	0.441610
		Steady-state error [%]	0.113363

Table 5.2 δ = 2° to - 2°

VOLTAGE MEASURES		CURRENT MEASURES	
Percent over-voltage [%]	5.172864	Percent overshoot [%]	126.333355
Time to achieve the over-voltage [s]	0.008002	Time to peak [s]	0.00775194
Settling time [s]	0.327332	Time to rise [s]	0.004001
Steady-state error [%]	0.787218	Settling time [s]	0.688922
		Steady-state error [%]	1.299649

CHAPTER 5

FEEDFORWARD / I_s – FEEDBACK CONTROL

5.1 Motivation

The central idea behind the implementation of a proportional control law is to determine the proportional constant. This chapter is concerned with the determination of the optimal gain constant, using the current error in order to make the corrective action over the parameter of control.

In order to analyze the influence of the negative feedback current-loop over the system's transient response, two structures of controls are defined. One structure uses δ as the parameter of control, while the other one uses μ. Each control scheme is based on a specific open-loop transfer function. The δ/μ feedforward /I_s-feedback to δ control uses the transfer function given by Equation (2.22), while Equation (2.23) is the base for the δ/μ feedforward /I_s-feedback to μ control.

The criterion to determine the optimal gain constant is set after a detailed root locus dynamical analysis of the open-loop transfer function of the system. Since the exact model does not have a mathematical expression for the reference current, an accurate equation is developed with the aid of the reactive current of the linearized average model. Each control configuration is implemented in both the exact and the average model. Finally, in order to estimate the performance measures, each model is submitted to step changes in current, from inductive to capacitive and vice-versa

5.2 Sampled and Average Compensator Current

As it was mentioned in the previous section, this type of control takes the current and feeds it back to modify the parameter of control δ or μ. The difference between the sampled and the reference current determines the amount of error. This error is then modified by the gain factor k, to adjust the parameter of control to a more adequate value. For the linearized averaged model the reference current is not a concern since the system is mathematically modeled, and therefore the behaviour of the system can be predicted using the equations developed in Chapter 2. On the other hand, the mathematical expression for the exact model can only be solved with the aid of a compute program.

The implementation of the control law in the exact model yields two major problems--one is to determine how and when to sample the current signal and the other is to find a mathematical expression that can be used to calculate accurately the reference current using the parameters δ and μ.

Creating a phase-locked loop between the current and the network voltage solves the first problem. This assures that the current is always sampled at the same position with respect to the network voltage. A careful look at the system in stationary condition (Figure 3.7) gives the right approach to solve the second problem since this value of the current is the reference value for this mode of operation. Therefore, the process to find all the reference values must be done under stationary conditions for all the parameters δ and μ.

Figure 3.7 also shows that the shape of the current signal depends on the compensator's mode of operation; this means that the moment of sampling is critical. Building a computer program to solve Equation (2.35) and to sample every cycle at the zero crossing of the network voltage yields the exact values for the reference current. These current values are plotted and then an equation that matches this curve is developed.

In order to see the correlation between these values and the ones given by the averaged model, both curves are shown in Figure 5.1. It turns out that modifying the equation of the average model in the way described below yields an expression that permits obtaining the reference current values with a high degree of precision.

$$Ia = A * Ic * \exp(B * \delta) - C$$

Where:

Ic reference current of the average model.

A=1.114, B=2.75 and C=8.38.

Figure 5.1, shows the current found by the average model, the current obtained from the exact model and the curve obtain with this mathematical expression. The graph clearly shows how well this equation matches the curve obtained by the exact model.

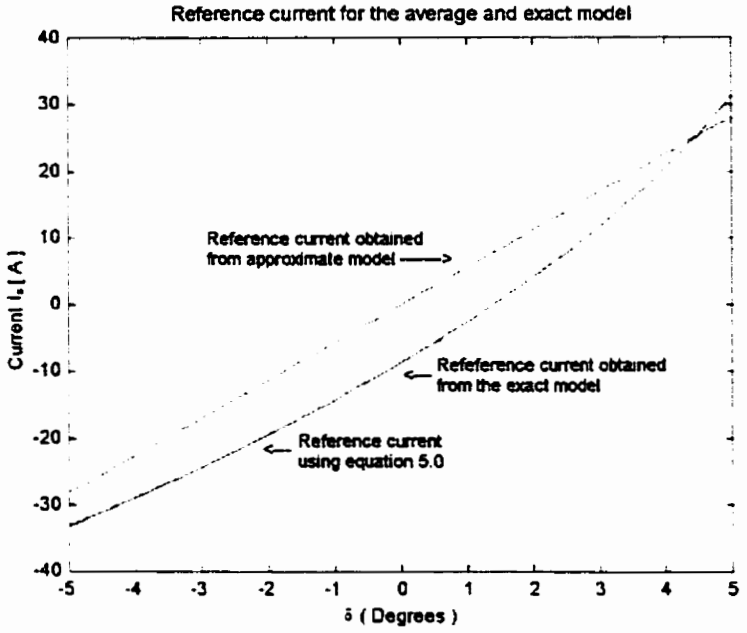

Figure 5.1. Reference current from average and exact model.

5.3 The δ / μ Feedforward / I_s – Feedback to δ Control

This section is concerned with the performance analysis of the feedforward/feedback scheme using phase-shift/pulse-width control. The parameter of control δ is adjusted proportionally to the difference between the reference current and the feedback current signal.

5.3.1 Control Structure

The δ/μ feedforward / I_s – feedback to δ control is shown schematically in Figure 5.2. The control structure for the exact model shows two positive feedforward-loops-- one for δ and the other for μ. The feedback current allows determining the magnitude of the current error and consequently modifying the parameter of control δ to a more adequate value by applying the proportional control law.

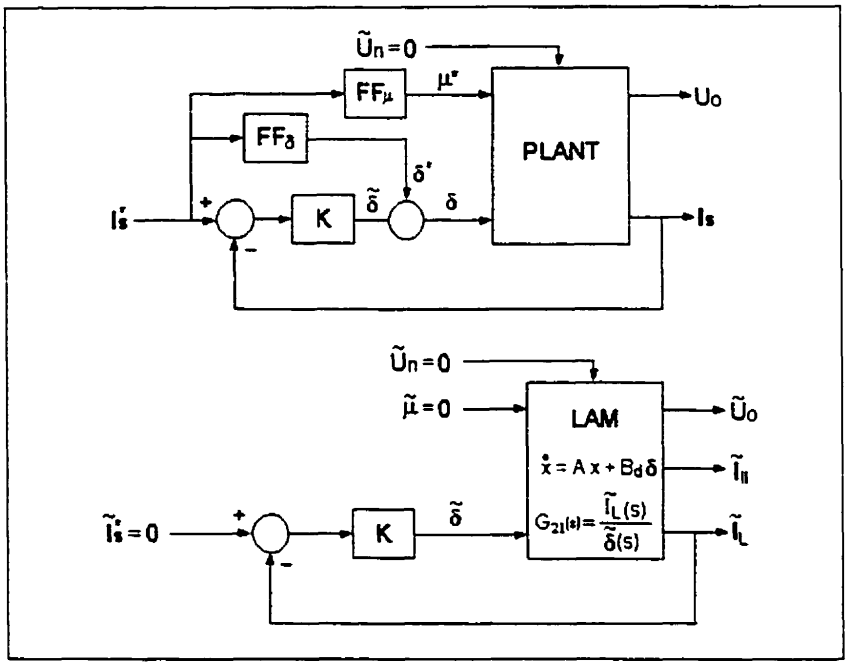

Figure 5.2. The δ/μ feedforward / Is – feedback to δ control implemented in the exact (top) and in the linearized average model (bottom).

For the average model, the open-loop transfer function of the control is given by Equation (2.22), which relates the variables δ and reactive current I_L. In the state space notation the $\mathbf{B_d}$ corresponds to the first column vector of the Jacobian matrix **B**. The

expressions for the control laws are given by Equations (5.1) and (5.2) for the exact and average model respectively.

$$\delta=\delta o + K(I_{s\_ref} - I_L) \quad (5.1)$$

$$\delta=-KI_L \quad (5.2)$$

5.3.2 Root Locus Dynamical Analysis

The open-loop transfer function of the δ / μ Feedforward / Is – Feedback to δ Control system given by Equation (2.22) determines the position of the open-loop zeros and the open-loop poles of the system in the s-plane. Since this equation is a function of the parameters δ and μ, then the open-loop zeros and the open-loop poles allocates in the s-plane accordingly to the values of these parameters. Figure 5.3 describes the movement of these open-loop zeros and the open-loop poles while δ and μ vary within all their operational values.

In order to facilitate the analysis, the location of the open-loop zeros in the s-plane, are represented in the graph by the lines united by a circle and a square. The circles show the pair of zeros when the system works at the maximum inductive mode, while the squares indicate the position at the maximum capacitive mode. The open-loop poles are represented by the lines united by an 'x' and a '*'. The 'x' show the open-loop poles when the system operates at the maximum inductive mode, while the '*' indicates the location at the maximum capacitive mode.

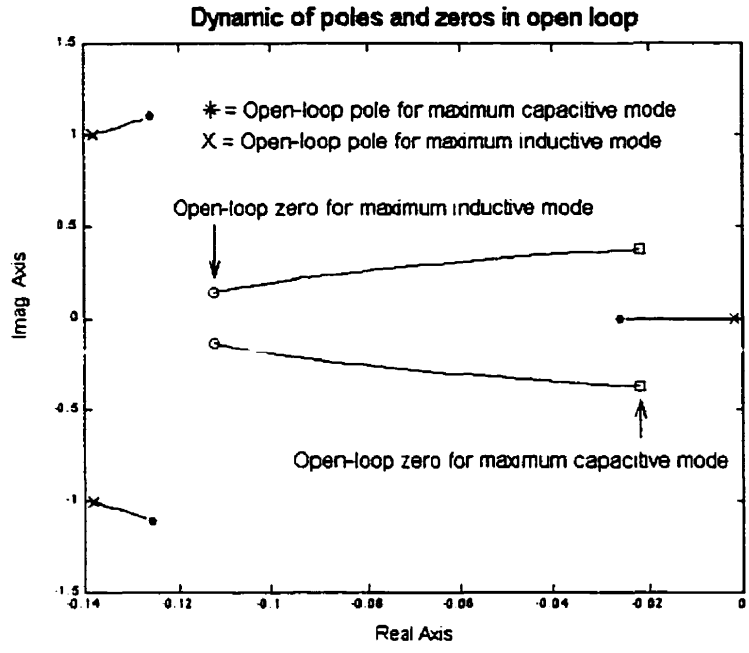

Figure 5.3. Dynamics of open-loop zero and open-loop poles, for the δ/μ feedforward / Is – feedback to δ control.

The figure shows that despite the mode of operation of the compensator, the angle contribution of the zeros to one of the complex open-loop poles is almost cancelled by the angle contribution of the remaining open-loop poles. This yields the determination that the angle of departure of the complex open-loop poles is around 180, regardless of the values of δ and μ. This figure also indicates that, despite the values of δ and μ, there is always one open-loop pole located over the negative side of the real axis. The exclusive and permanent location of this open-loop pole assures that the section of the real axis between minus infinity and this pole is always a branch of the root locus. Therefore, considering all the above statements the dynamics of the root locus can be established. Initially all the closed-loop poles travel to minus infinity as the gain increases, but since the open-loop zeros define the termination of the root locus, and this must be symmetrical to the real axis, the following must take place. The conjugate

closed-loop poles will converge at a point over the negative side of the real axis and then one closed-loop pole travels left, while the other one travels right. The closed-loop pole that travels to the right meets now with the real closed-loop pole that has been travelling left; at the point of convergence, one pole will travel toward the zero above the real axis while the other travels to the zero below the real axis. Figures 5.4 confirm the above statements.

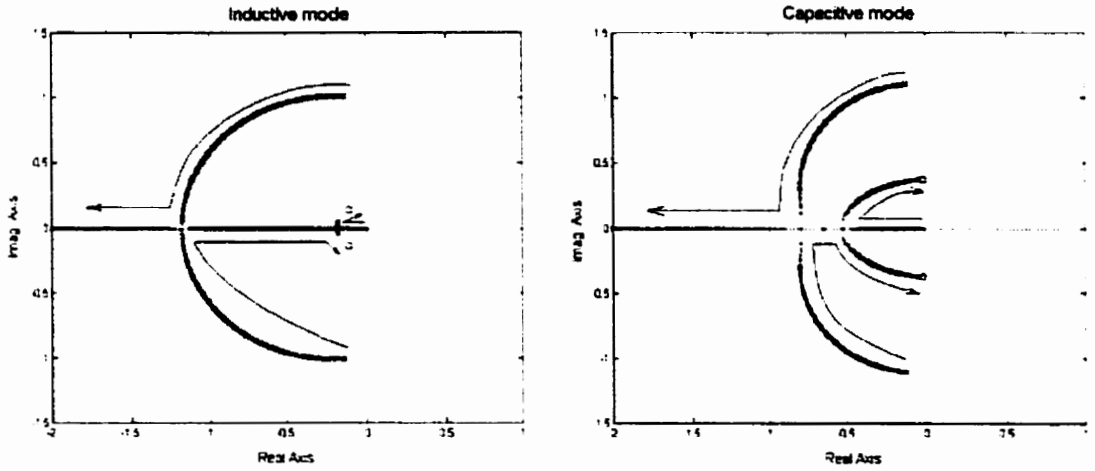

Figure 5.4. Typical Root locus of the compensator system in inductive mode (left) and in capacitive mode (right).

5.3.3 Optimal Gain Determination

Figure 5.4 shows that the system is stable for all values of δ and μ. Therefore, the issue of stability is not a concern in this particular control structure and thus from this point of view, there is no restriction for the gain. This figure also shows that initially all the closed-loop poles move away from the imaginary axis until the point of convergence of the complex conjugate closed-loop poles. Hence this point of convergence will serve as

the first attempt to find the optimal gain. Figure 5.5 show the values of the gain at each point of convergence.

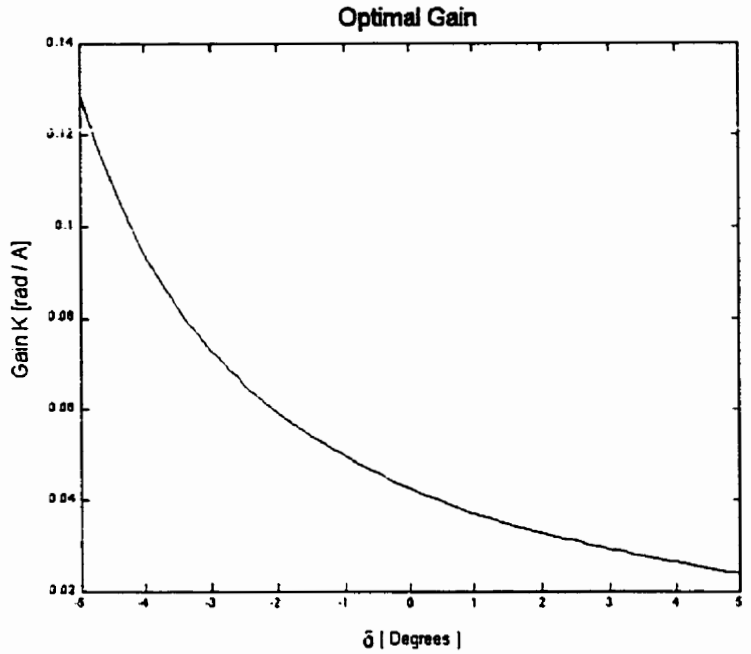

Figure 5.5. Gain for each point of convergence of the complex poles.

The above figure shows that the optimal gain for the system can be set to 0.127 rad/A. Nevertheless, the use of excessive gain may cause the system to operate in its non-linear regime or out of the system restrictions; therefore, a value of 0.0239 [rad/A] will show to be adequate.

The dynamics of the whole system, when the optimal gain is set to 0.0239 rad / A is depicted by Figure 5.6. The points highlighted in the graph by an "x" denote the maximum inductive operating mode of the compensator. As the compensator moves to its capacitive mode, the conjugate, closed-loop poles of the system move away to the left

from the imaginary axis and closer to the real axis. This suggests that the system will have a higher percent overshoot when the step change in reactive current is made from capacitive to inductive. Even though the behaviour of the conjugate, closed-loop zeros have an opposite effect than the conjugate closed-loop poles, the latter behaviour of the closed-loop poles prevail. Since the percent overshoot is expected to be higher for the step change from capacitive to inductive, the settling time is also expected to be higher.

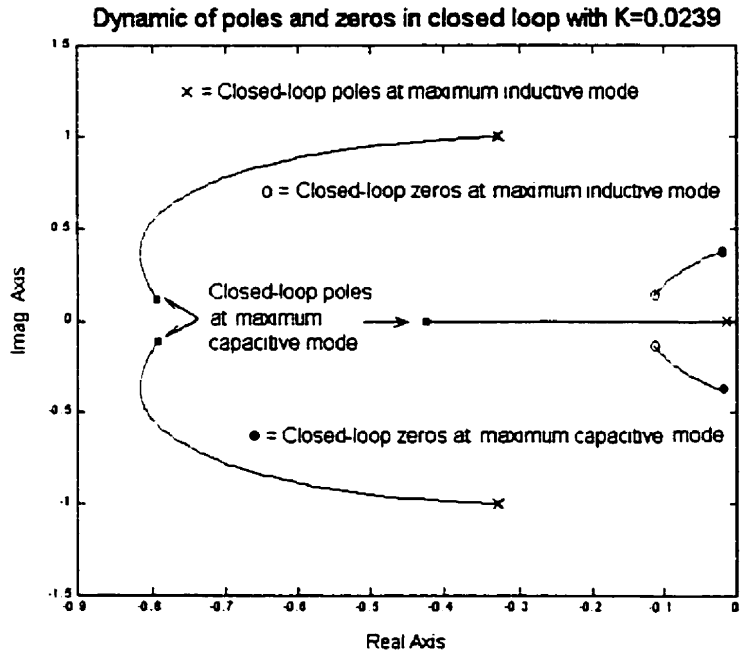

Figure 5.6. Dynamic behaviour of the whole system when the optimal gain is set to 0.0239 rad/A.

5.3.4 LAM Response

Figure 5.7 describes the performance of the linearized average model of the compensator when submitted to a step change in reactive current, from inductive to capacitive and vice-versa. Notice that the system response is very fast and that the percent overshoots are small compared with the other control structures analyzed so far. The response in

Figure 5.7 corresponds to a step change from 11.311A peak inductive to 11.311A peak capacitive, and vice-versa.

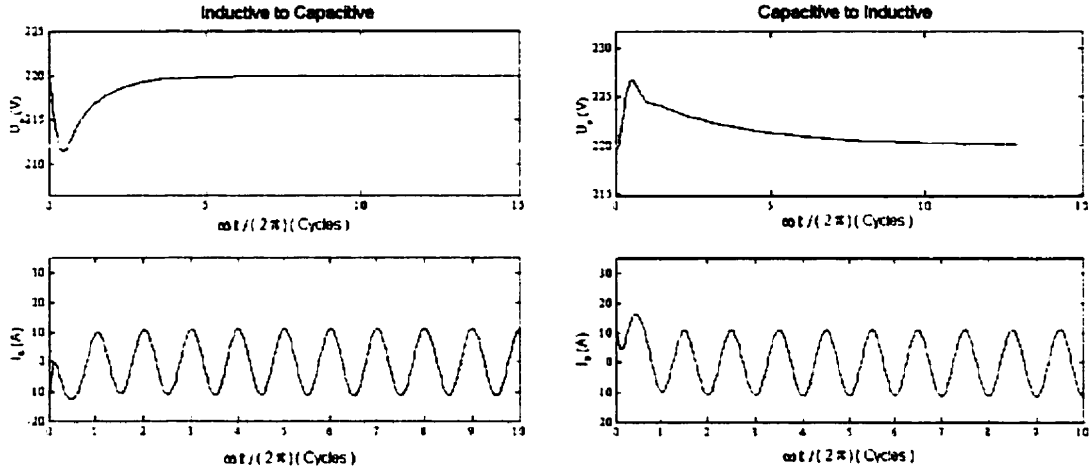

Figure 5.7. Linearized average model response for a step change from inductive to capacitive (left) and vice-versa. When the δ / μ feedforward / Is – feedback to δ control is implemented in the average model.

5.3.5 Exact Response and Comparison with the LAM Response.

The left side of Figure 5.8 depicts the exact model response to a step change in reactive current from inductive to capacitive, while the right side describes the response to the opposite change. The responses correspond to changes in reactive current from 11.311A peak inductive to 11.311A peak capacitive, and vice-versa.

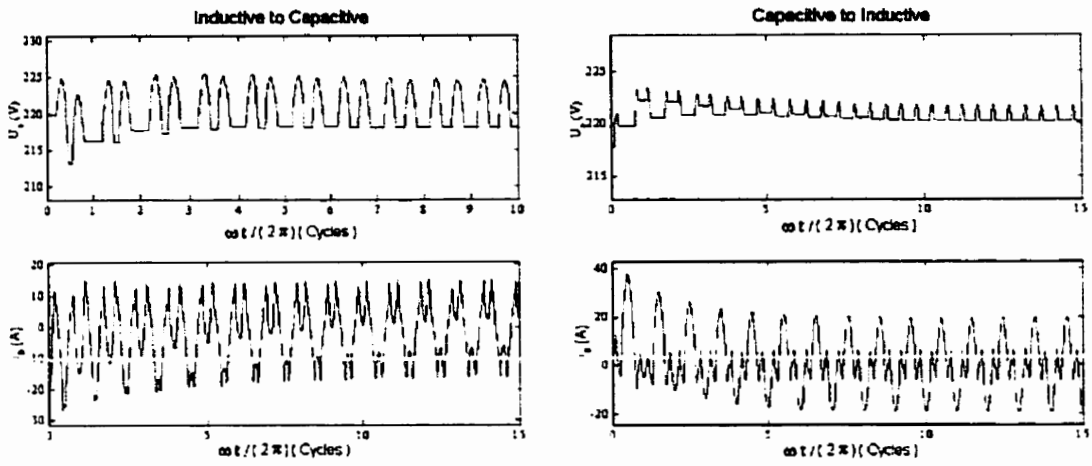

Figure 5.8. Exact model response for a step change from inductive to capacitive (left) and vice-versa. When the δ / μ feedforward / Is – feedback to δ control is implemented in the average model.

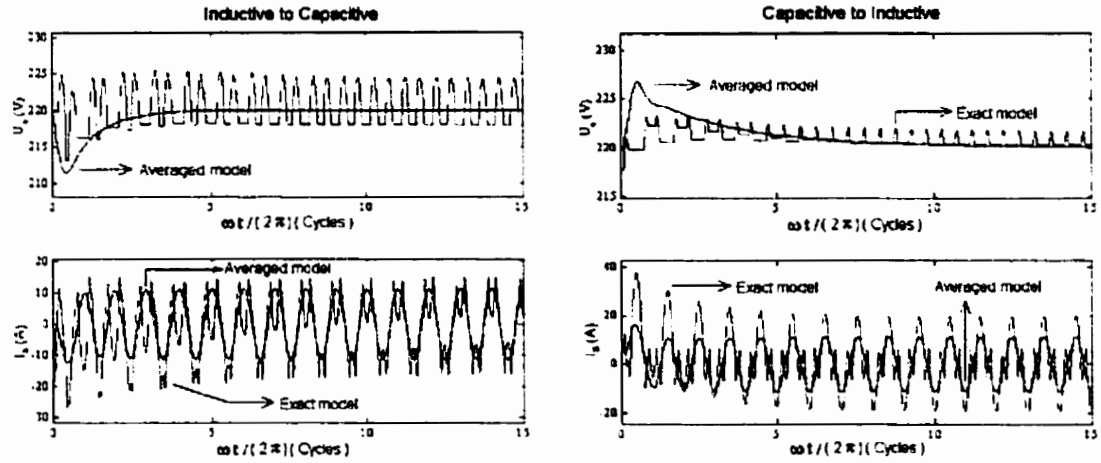

Figure 5.9. Exact and average model responses for a step changes from inductive to capacitive (left) and vice-versa. When the δ / μ feedforward / Is – feedback to δ control is implemented in the both models.

5.3.6 Performance Measures

The evolution of the reactive current during the transient from inductive to capacitive and vice-versa is described in Figure 5.10. Notice that there is no oscillation in either transient and that the response is so far the fastest. The voltage variation is also the

smallest and the percent overshoot is among all the control structures analyzed by now, the smallest.

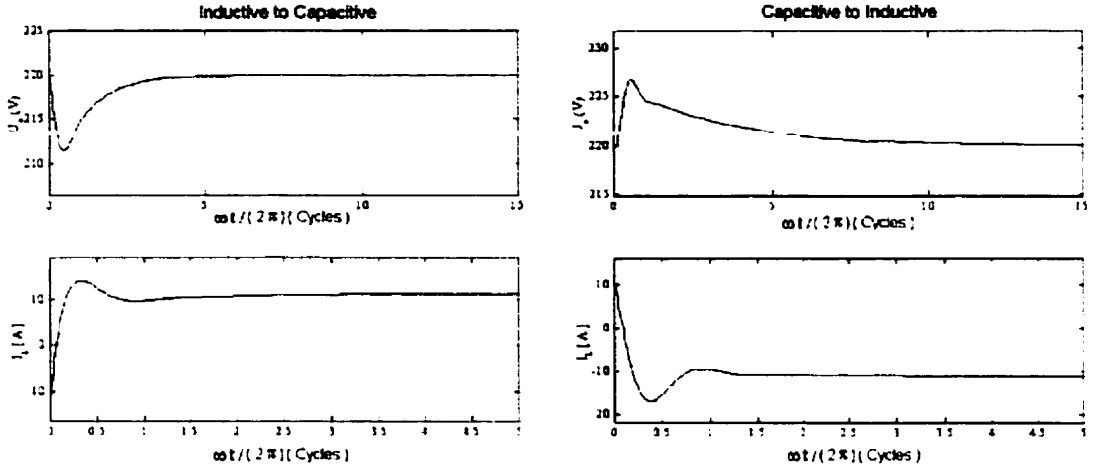

Figure 5.10. Step change in reactive current from inductive to capacitive and vice-versa.

Table 5.1 δ = - 2° to 2°

VOLTAGE MEASURES		CURRENT MEASURES	
Percent over-voltage [%]	3.900649	Percent overshoot [%]	24.978728
Time to achieve the over-voltage [s]	0.007502	Time to peak [s]	0.0052513
Settling time [s]	0.01875	Time to rise [s]	0.00300
Steady-state error [%]	0.00	Settling time [s]	0.0475
		Steady-state error [%]	0.00

Table 5.2 δ = 2° to - 2°

VOLTAGE MEASURES		CURRENT MEASURES	
Percent over-voltage [%]	3.055172	Percent overshoot [%]	49.783942
Time to achieve the over-voltage [s]	0.008752	Time to peak [s]	0.006252
Settling time [s]	0.018255	Time to rise [s]	0.003251
Steady-state error [%]	1.2*10^-8	Settling time [s]	0.071768
		Steady-state error [%]	3.262672

5.4 The δ / μ Feedforward / Is – Feedback to μ Control

5.4.1 Control Structure

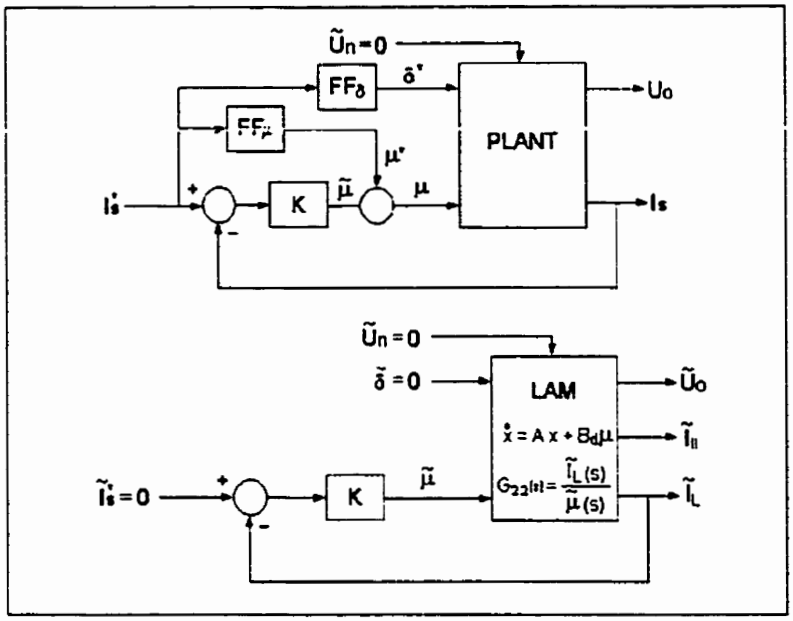

Figure 5.11. The δ/μ feedforward / Is – feedback to μ control implemented in the exact (top) and in the linearized average model (bottom).

The δ/μ feedforward / Is – feedback to μ control is shown schematically in Figure 5.11. The control shows two positive feedforward-loops-- one for δ and the other for μ. The negative feedback current-loop allows determining the magnitude of the error and consequently modifying the parameter of control μ to a more adequate value by the proportional control law. For the average model, the open-loop transfer function of the control is given by Equation (2.23), which relates the variables μ and reactive current I_L. The expressions for the control laws are given for the exact and average model as follows:

$$\mu=\mu_o + K(I_{s\_ref}-I_s) \quad (5.3)$$

$$\mu=-KI_s. \quad (5.4)$$

5.4.2 Root Locus Dynamical Analysis

The open-loop transfer function of the δ/μ feedforward / I_s – feedback to μ control system given by Equation (2.23) determines the position of the zeros in the s-plane. Since the numerator of this expression is a function of the parameters δ and μ, then each pair of zeros allocates in the s-plane accordingly to the values of these variables. Figure 5.12 describes the movement of these zeros while δ and μ vary within all their operational values. In order to facilitate the analysis, the zeros are represented in the graph either by a square or by a circle. In this figure, the projection of each zero over the horizontal axis gives the actual position of the zero in real axis of the s-plane; on the other hand, the projection of the same zero over the vertical axis determines the mode of operation in which the compensator in working.

In the inductive mode, for values of $\delta<0$, the zero represented by the square lies always on the right hand side of the s-plane and moves to infinity as the inductive current decreases to zero. Now, since this zero determines the end of one branch of the root locus, one of the closed-loop poles will reach this zero as the gain increases. For a particular value of the gain, this pole will cross the imaginary axis of the s-plane, resulting in an unstable system. Therefore, under this mode of operation, at one point, the system will become unstable.

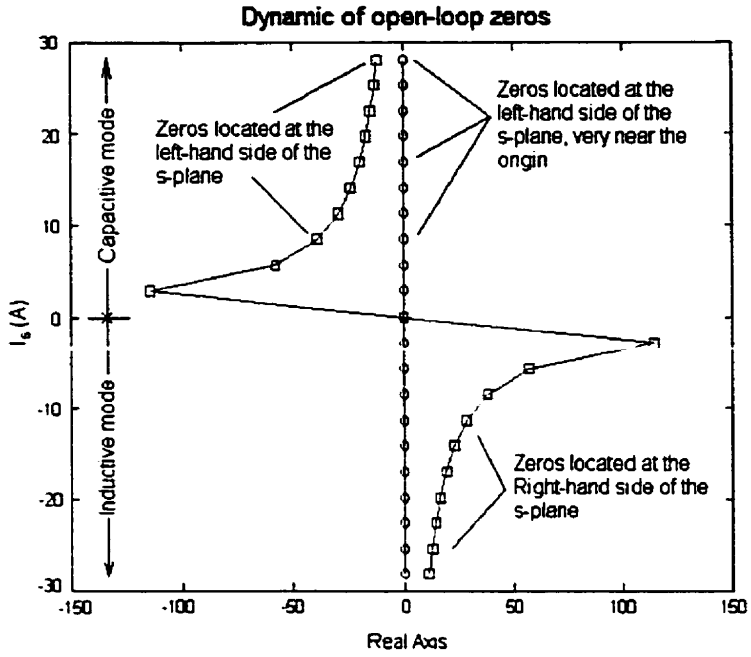

Figure 5.12. Zeros dynamic as the δ and μ change.

In the capacitive mode, for values of $\delta>0$, this zero lies always on the left-hand side of the s-plane and moves to minus infinity as the capacitive current decreases to zero. Since this zero is always over the real axis on the left-hand side of the s-plane, its dynamical position will not cause unstability, as the closed-loop poles approach this zero.

This figure also shows that for this open-loop transfer function, independent of the mode of operation of the compensator, there is always one zero located extremely near the origin of the s-plane. This is an undesired position for a zero, since it will create a slow closed loop pole that will cause a long transient response and an increase in the percent overshot. Nevertheless, this will also depend on how close is the traveling closed-loop pole to this zero at a given gain, and its relative position with the other poles. A particular mode of operation that deserves a close look results when $\delta=0$. An analysis of

Equation (2.23), shows that for this particular condition, the numerator reduces to polynomial of a first order of the type $C_1*s=0$, therefore, on this mode of operation, the system has only one zero located at the origin.

The poles of the open-loop transfer function determine the starting point of the root locus. The position of these poles depends on the value of the parameters δ and μ. Figure 5.13 shows the movement of these poles while δ and μ vary within all their operational values, it also shows the direction of departure of the most relevant poles. In this figure, the position of the one pole of the open-loop transfer function is evaluated for one specific value of δ and μ.

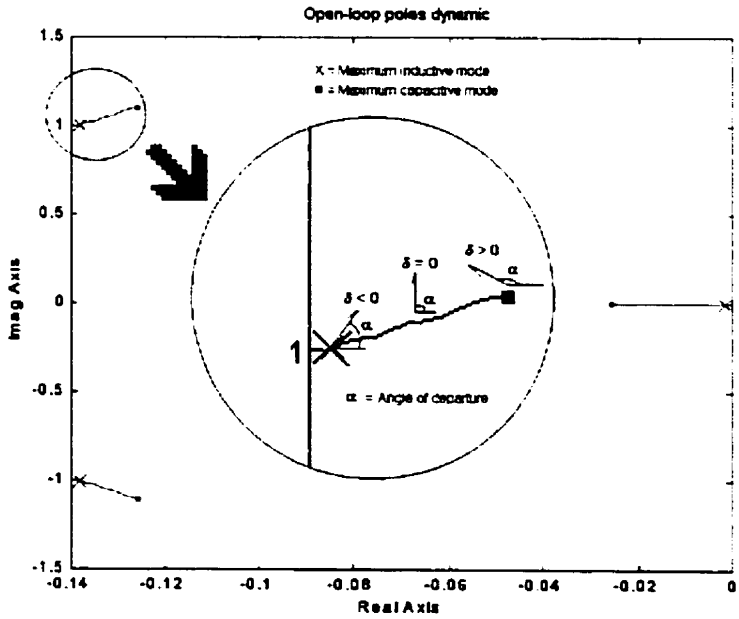

Figure 5.13. Poles dynamic as δ and μ change.

In the inductive mode, there is always one zero on the right hand side of the s-plane. Therefore, the upper complex open-loop pole depicted in the figure by an 'x' will be the

starting point of one branch of the root locus. The closed-loop poles will follow the direction of the arrow as the gain increases. Since the root locus must be symmetrical with respect to the real axis, the other complex open-loop pole will be the starting point of other branch of the root locus. These two poles travel to the right hand of the s-plane, and will meet at a point to the right of the zero located over the positive side of the real axis. For greater values of the gain the closed-loop poles will travel along the real axis but in opposite direction-- one toward the zero and the other one to plus infinity. Figure 5.14, shows a typically root locus of the system in the inductive mode for one unique set of value of the parameters δ and μ.

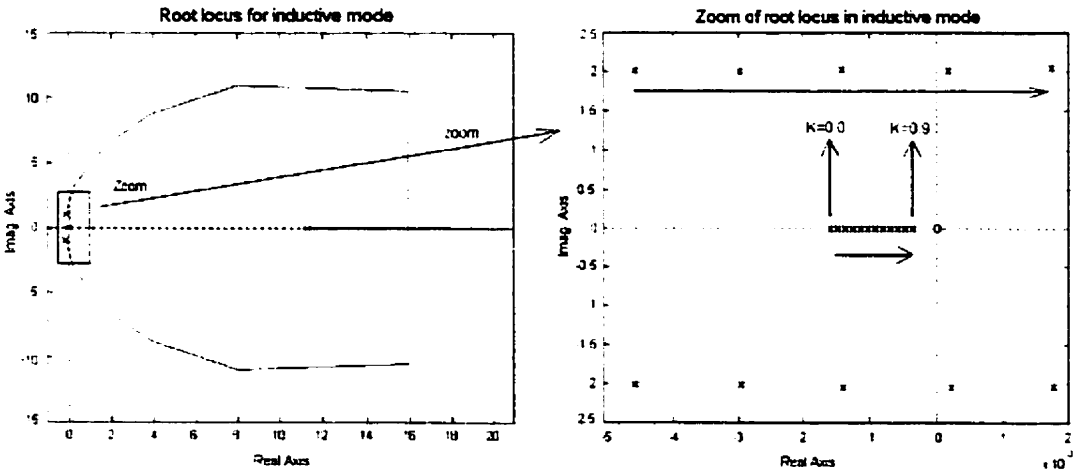

Figure 5.14. Typical Root locus of the system in inductive mode, $\delta<0$.

As δ increases and approaches zero, two important and opposite things will happen. On one hand, the open-loop poles get closer to the imaginary axis and therefore, the closed-loop poles reach the imaginary axis with smaller values of the gain. On the other hand, the zero located in the right-hand side of the s-plane moves further to plus infinity, causing an increment in the angle of departure. As a result of this increment, now each

time the closed-loop poles will reach the imaginary axis for bigger values of the gain; in the limit, when $\delta=0$, the angle of departure reaches 90 degrees and the system is always stable regardless of the value of the gain. The latter effect over the gain is stronger than the former. This result suggest that the maximum inductive mode of operation gives the worst case scenario to determine the maximum value of the gain for the system to remain stable for all values of δ and μ. Figure 5.15 shows the motion of the closed-loop poles for this case.

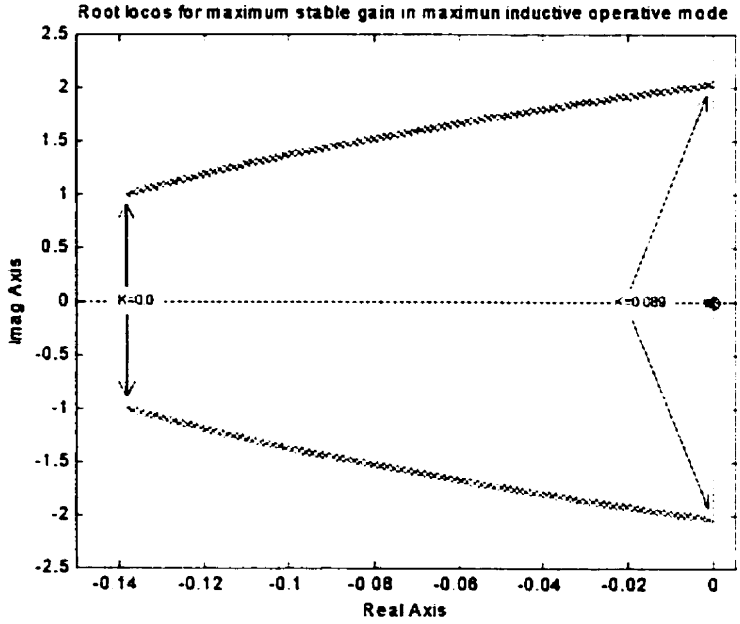

Figure 5.15. Root locus for maximum inductive operative mode with gain range from of 0 to 0.089 rad/V.

The behaviour of the real pole is quite simple and is described in Figure 5.13. As δ increases, from the maximum inductive mode of operation to the maximum capacitive operative mode, the real open-loop pole starts further to the left of the origin; but as the gain increases, the closed-loop pole always travels to the right toward the zero located

almost statically at the origin. In the capacitive mode, the zero is always over the real axis on the left-hand side of the s-plane. Therefore, the closed-loop conjugate poles travel now to the left, toward the zero that lies on the negative side of the real axis; this time they meet at a position to the left of the zero. Beyond the point of convergence, the poles travel along the real axis as the gain increases, but one travels to minus infinity while the other one goes toward the zero. In this mode of operation, there is no restriction on the gain since the system remains stable independent of the value of this variable. Figure 5.16, shows a typical root locus of the system in the capacitive mode for one unique value of the parameters δ and μ.

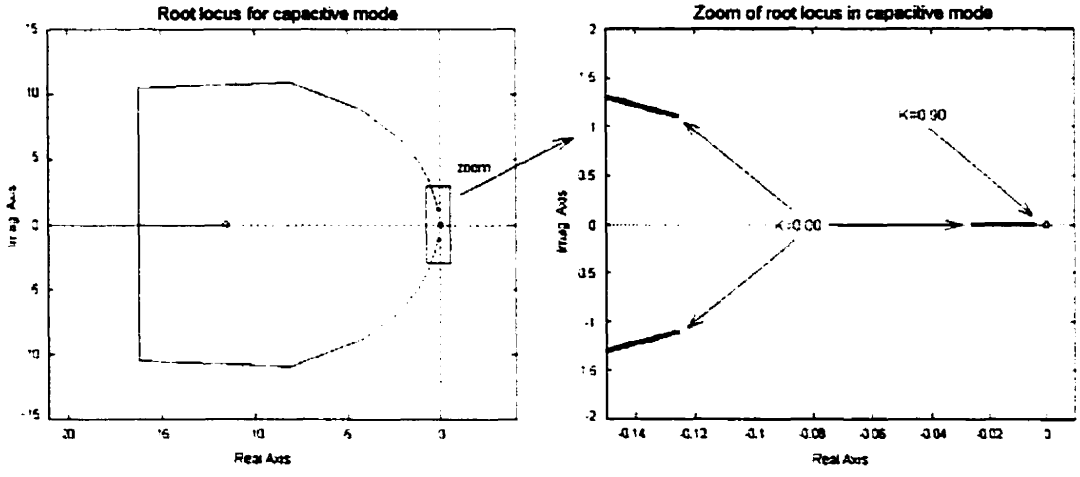

Figure 5.16 Typical Root locus of the system in capacitive mode, $\delta<0$

5.4.3 Optimal Gain Determination

It was established before, that the maximum inductive operative mode gives the worst case scenario to determine the maximum gain for the system to remain stable under all circumstances. The gain value for this condition was found to be k = 0.089 rad / V, which is relatively high but since high levels of gain improve the steady-state error, disturbance response, parameter sensitivity and dynamic response, it seems to be

reasonable to use this number as the optimal gain. Nevertheless a further analysis is required before setting this value as the optimal gain. Figure 5.17 shows the dynamics of the closed-loop poles when k=0.089 and δ and μ change within their operational values. This graphs also shows that in the inductive mode, for some values of δ and μ, the closed-loop poles are extremely close to the imaginary axis, thus compromising the stability of the system. On the other hand, the use of excessive gain may cause the system to operate in its non-linear regime or out of the system restrictions. According to the control law if k=0.089 rad / V is taken as the optimal gain a step change in reactive current from 11.3A in capacitive mode to 11.3A in inductive mode, will cause an output value of δ=211.100, which by far exceeds the upper limit of δ. Thus, these results suggest a different criterion is needed to find the optimal gain.

A closer analysis of Figure 5.13 suggests the right criterion. The figure shows how the open-loop poles behave as the system operates from its maximum inductive operation mode to its maximum capacitive operative mode. In the inductive mode, the open-loop poles are further left than the open-loop poles in capacitive mode, but as gain increases, the closed-loop poles move in opposite directions.

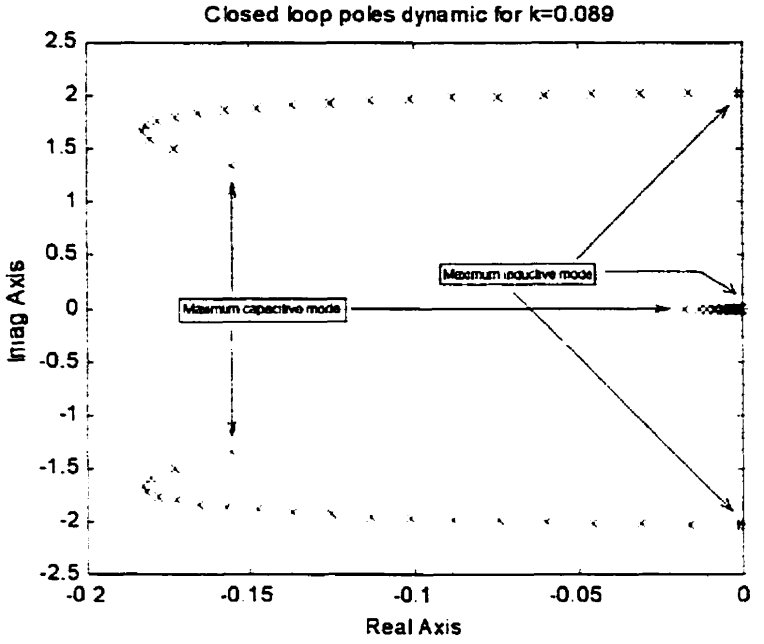

Figure 5.17 Closed loop poles dynamic for k=0.089.

Consequently in the inductive mode, the closed-loop poles will get closer to the imaginary axis as the gain increases, while in the capacitive mode these poles will move away from the imaginary axis. Thus the gain must be high enough to let the closed-loop poles in capacitive mode move away from the imaginary axis, but low enough to avoid the closed-loop poles in the inductive mode to get to close to the imaginary axis.

Figures 5.18 shows the dynamic of one of the two conjugate poles for specifics values of the gain when the parameters μ and δ vary along their operational values. For k=0.005, the closest pole lies slightly to the right of –0.128; for k=0.006 the closest pole lies slightly to the left of –0.128 and for a gain of k=0.007 the closest pole lies slightly to the left of –0.127.

From this graph, it can easily be seen that k=0.006 gives the optimal value of the gain. This gain permits to maintain all the closed-loop poles are far from imaginary axis. At this point, it is important to note that even though, this is the best choice, these poles still lie to close too the imaginary axis and thus an oscillatory behaviour is expected for a step change in current, as well as high percent overshot and high settling time.

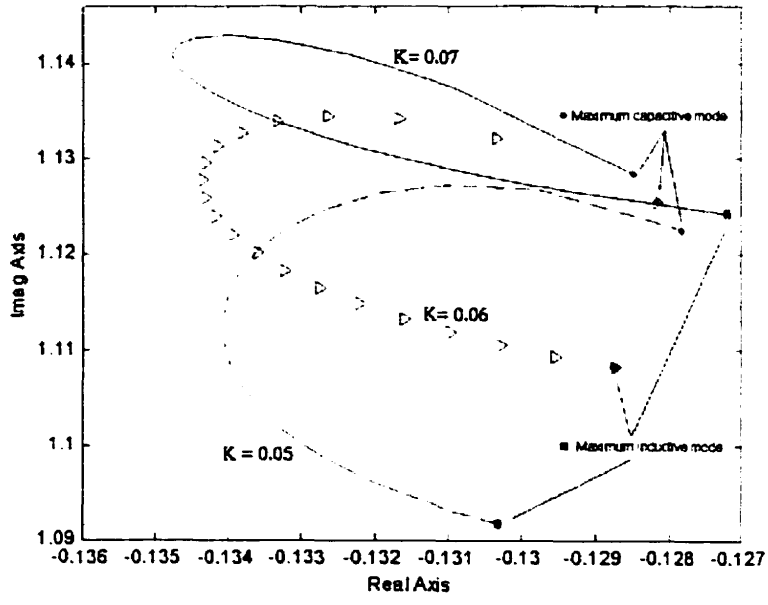

Figure 5.18. Dynamic of the upper complex closed-loop pole for different gains.

5.4.4 LAM Response

Figure 5.19 shows the linearized averaged model response to a step change in current from 11.311 A peak inductive to 11.311 A peak capacitive. The upper part of this figure shows a large transient on the voltage; this is due to the slow pole located near the origin, as was pointed before on previous sections. In the first cycle, the voltage drops from 220 V to 203 V, and oscillates for about five cycles before it starts to increase with a slow

exponential toward the 220 V. The control takes about 8 cycles to recover the voltage to its 97.7 %. This is to 215 V. The maximum voltage drop is less than 8%.

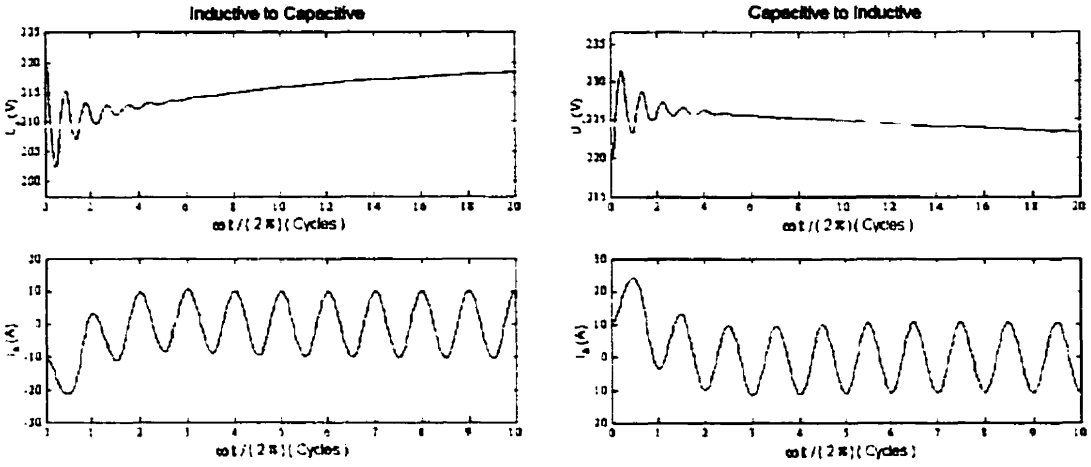

Figure 5.19. Linearized average mode responses for step changes in reactive current from inductive to capacitive (left) and vice-versa.

The lower part of this figure shows the behaviour of the current for this contingence. The current initially drops to –21 A, but within the first 4 cycles, it almost recovers its desired value. It is important to note that there is almost no distortion in the shape of the current curve, for this step change.

5.4.5 Exact Response

Figure 5.20 shows the exact model response to a step change in current from 11.311 A peak inductive to 11.3111 peak capacitive. The upper part of this figure shows a large transient on the voltage; this is due to the slow pole located near the origin, as was pointed out before and confirmed by the average and now by the exact model. In the first cycle, the voltage drops from 220 V to 189.5 V, and oscillates for about five cycles

before it starts to increase with a slow exponential toward the 220 V. The control takes about 10 cycles to recover the voltage to its 97.7 %. This is to 215 V. The maximum voltage drop is less than 14%. It is important to keep in mind that the average model does not consider all the non-liberties, while the exact model does.

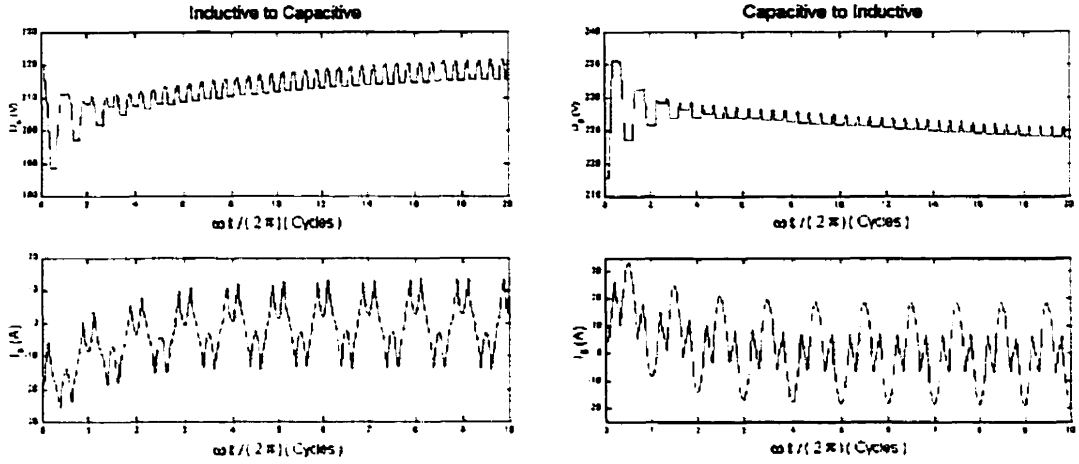

Figure 5.20. Exact model responses to step changes from inductive to capacitive (left) and from capacitive to inductive.

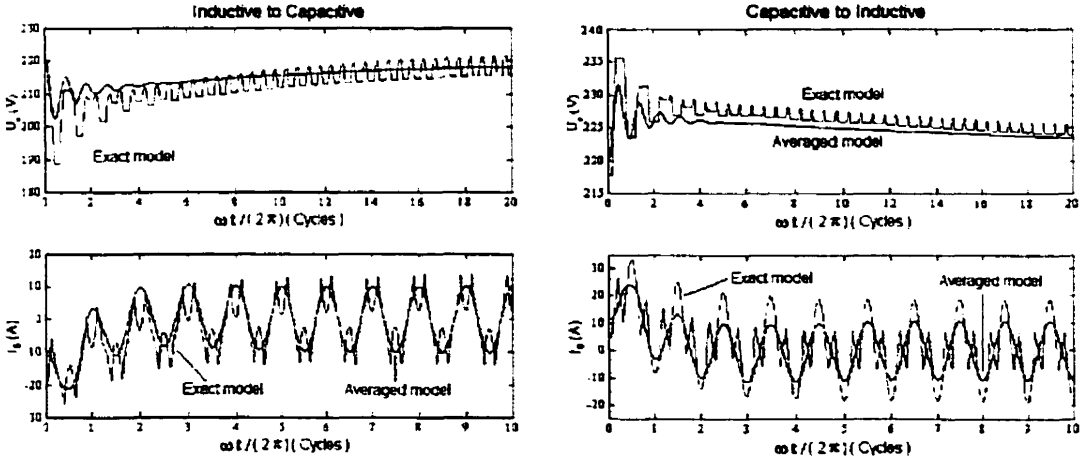

Figure 5.21. Dynamic response of the compensator to a step change in current from 11.311A peak inductive to 11.31 A peak capacitive, achieved with the average and the exact model.

The lower part of this figure shows the behaviour of the current for this step change. The current initially drops to a peak value of approximate –25 A, but within the first 4 cycles, it almost recovers its desired value. It is important to note that for the exact model there is also almost no distortion of the shape of the current curve, for this step change. Figure 5.21, shows the behaviour of the two models. It can easily be seen that the average model is indeed a very good representation of the exact model, even though it does not takes into consideration the non-linearities of the system.

5.4.6 Performance Measures

The performance of the compensator to step changes using the δ / μ feedforward / Is – feedback to μ control is depicted in Figure 5.22. Tables 5.3 and 5.4 summarize the estimation of the performance measures.

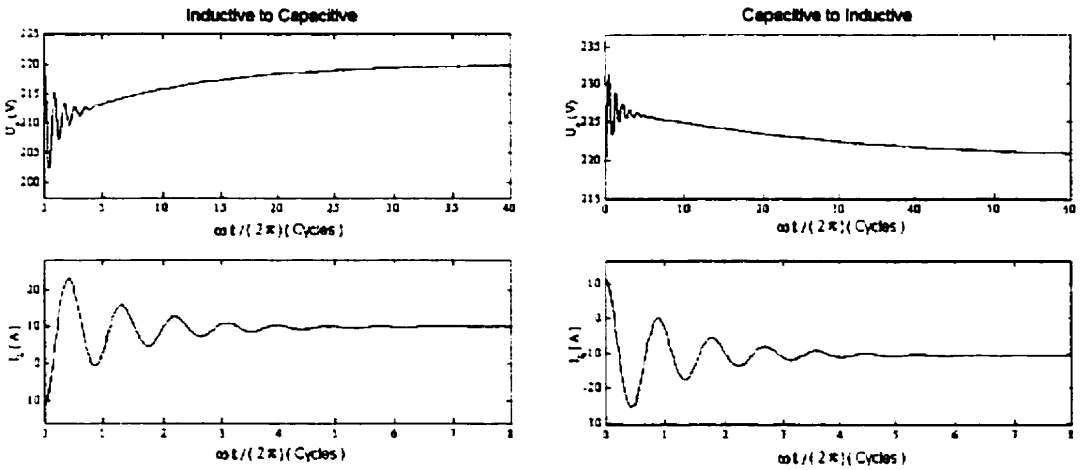

Figure 5.22. Current and voltage performance of the compensator, when submitted to step changes in reactive current and using the δ / μ Feedforward / Is – Feedback to μ Control.

Table 5.3 δ = - 2° to 2°

VOLTAGE MEASURES		CURRENT MEASURES	
Percent over-voltage [%]	7.597273	Percent overshoot [%]	104.8803
Time to achieve the over-voltage [s]	0.007252	Time to peak [s]	0.007002
Settling time [s]	0.159790	Time to rise [s]	0.003751
Steady-state error [%]	0.019652	Settling time [s]	0.425106
		Steady-state error [%]	0.084583

Table 5.4 δ = 2° to - 2°

VOLTAGE MEASURES		CURRENT MEASURES	
Percent over-voltage [%]	5.221592	Percent overshoot [%]	128.154858
Time to achieve the over-voltage [s]	0.0072518	Time to peak [s]	0.0072518
Settling time [s]	0.219805	Time to rise [s]	0.003751
Steady-state error [%]	0.413257	Settling time [s]	0.66067
		Steady-state error [%]	1.00754

CHAPTER 6

FINAL REMARKS

6.1 Conclusions

There are many possible schemes to control an inverter-based compensator. In this investigation, a total number of 7 different control structures have been analyzed, evaluated and compared. These structures have shown a fairly large difference in terms of dynamic performance. The simulation results indicate that the best dynamic performance is achieved with the δ/μ feedforward /Is-feedback to δ control. The main benefit of this structure is its low percent overshoot in voltage in current, but it is also registers the lowest steady state error and fastest transient response (i.e., lowest settling time)

This research has shown that by introducing another variable of control to vary the width of the square wave generated by the switching devices, it is possible to maintain a unique constant inverter voltage value over the operating range of interest.

The Jacobian of the linearized average model allowed the discovery of the systems' high degree of coupling and thus avoided analysis of structures with a double feedback loop. This linearized average indicated that it is not only very useful for control synthesis but, it is also appropriate to represent the fundamental frequency behaviour of the compensator in stationary and dynamic conditions.

This work has shown that with the appropriate modelling and detailed analysis it is possible to achieve good performance of the inverter-based compensator by implementing a simple control structure with just a proportional control law. The critical and optimal gains, determining the dynamics of the system, comprehending the behaviour of the compensator and even predicting the response of the system to step changes in reactive current from one mode of operation to another.

In addition, this study verifies through the simulations that the developed equations in order to find the reference value for voltage and current are indeed the appropriate values. It also reveals that it is better to control the phase-shift (variable δ) instead of the pulse-width (variable μ). Finally the methodology used in this work can serve as a basis for analyzing future compensation models.

6.2 Recommendation For Future Work

The expansion of this work will involve the following aspects:

1. Decouple the system in order to avoid the interaction between the input and output variables. Decoupling will allow the implementation of double feedback loops to independently control each input.
2. Analyze the impact of the delay in the feedback loop of the δ/μ feedforward /Is-feedback to δ control and investigate its influence over the stability of the system.
3. Implement the δ/μ feedforward /Is-feedback to δ control in the actual laboratory prototype built in the previous investigation [1].
4. Allocate the closed-loop poles to a desired position by using the pole placement procedure and investigate the behaviour of the control structures analyzed in this thesis.

References

[1] Yihui Zhang, "DSP-Based Control Strategies For An Inverter-Based Compensator," Master of Science Thesis, University of Manitoba, Winnipeg, February 1999.

[2] George C. Verghese, Marija Ilic-Spong, Jeffrey H. Lang, "Modelling And Control Challenges In Power Electronics,", Proceedings of the 25th Conference on Decision ans Control, Athens, Greece, December 1986.

[3] Brian K. Perkins, "Dynamic Modelling Of An Inverter-Based Compensator," presented at the 1999 IEEE Power Electronics Specialist Conference, Charleston, SC, June 27-July 1 1999.

[4] Seth R. Sanders, George C. Verghese, Derrick F. Cameron, "Nonlinear Control Laws For Switching Power Converters," Proceedings of the 25th Conference on Decision ans Control, Athens, Greece, December 1986.

[5] H.R. Visser, P.P.J. van den Bosch, "Modelling of Periodically Switching Networks," IEEE PESC Record, pp. 67-73, 1991.

[6] S. Sanders, J. Noworoski, X. Lui and G. Verghese, "Generalized Averaging Method For Power Conversion Circuits," IEEE Power Electronics Specialist Conference (PESC), San Antonio, June 1999, pp. 333-340.

[7] M. Sonnenschien, M. Weinhold, and R. Zurowoski, "Shunt-Connected Power Conditiones For Improvement Of Power Quality in Distribution Networks," Proceedings of the 7th International Conference on Harmonics and Quality Of Power, October 16-18 1996.

[8] M. Jamshid, M Malek-Zavarei, "Linear Control Systems, A Computer Aided Approach," Volume 7, Pergamon Press 1986.

[9] John Van de Vegte, "Feedback Control Systems." Prentice-Hall 1986.

[10] A. Frank D'Sousa, "Desing Of Control Systems," Prentice-Hall 1988.

[11] Richard C. Dorf and Robert H. Bishop "Modern Control Systems," 8th Edition Addison-Wesley. 1998

[12] Katsuhiko Ogata, "Modern Control Engineering," Prentice-Hall 1986.

[13] MATLAB Version 5 User's Guide.